CHAPTER 1

Density-Functional Theory of *sp*-Bonded Defects in III/V Semiconductors

Udo Scherz

FACHBEREICH PHYSIK, TECHNISCHE UNIVERSITÄT BERLIN
BERLIN, GERMANY

Matthias Scheffler

FRITZ-HABER-INSTITUT DER MAX-PLANCK-GESELLSCHAFT
BERLIN, GERMANY

ISBN 0-12-752138-0

I. Introduction

The requirements of semiconductor technology for accurate control of defect concentrations, concentration profiles, defect electronic structure, diffusion properties, formation and reaction energies, and atomic structures at interfaces has stimulated extensive experimental and theoretical research. Several exciting new phenomena have been discovered throughout these investigations, as for example the "negative U" property of the vacancy in silicon (Baraff *et al.*, 1979, 1980; Watkins and Troxell, 1980), i.e., an effective electron–electron attraction; and the *EL2* (Martin and Makram-Ebeid, 1986; Dabrowski and Scheffler, 1988a, 1989a; Chadi and Chang, 1988a) and *DX* (Chadi and Chang, 1988b; Zhang and Chadi, 1990; Dabrowski *et al.*, 1990; Dabrowski and Scheffler, 1992) metastabilities, which demonstrate the capability of the III/V crystal to stabilize defects in different atomic configurations (Scheffler, 1989; Caldas *et al.*, 1990; Dabrowski and Scheffler, 1992). These and many more examples, as well as the discussions and controversies in the process of unveiling the underlying physics, show that the *basic* understanding of many-particle effects in condensed-matter science, and in particular for low-symmetry polyatomic aggregates, as for example defects in semiconductors, is still rather limited.

The derivation of density-functional theory (DFT) (Hohenberg and Kohn, 1964; Kohn and Sham, 1965; Levy, 1982), together with the local-density approximation (LDA) for the exchange-correlation functional (Dreizler and Gross, 1990; Lundqvist and March, 1983; Ceperley and Alder, 1980; Perdew and Zunger, 1981) has played a significant role in improving this situation, and DFT-LDA will certainly still play an important role in the coming years. This theory describes the electronic ground state and contains all many-electron effects of the nonrelativistic interacting many-body systems of constant and weakly varying densities. For very inhomogeneous densities and for highly localized electron states (as, for example, in free atoms), the DFT-LDA is not a reasonably defined approximation for the treatment of exchange and correlation. This criticism, although certainly valid in principle, has not stopped theoreticians from applying this approach to calculate structural and elastic properties of polyatomic systems. The demonstrated success of the theory (e.g., Moruzzi *et al.*, 1978; Cohen, 1985) is in fact overwhelming, and no *severe* breakdown of the theory has been reported so far (see Section III.4 for more details). We like to emphasize at this point that an accurate evaluation of the DFT-LDA electron density and total energy is usually very difficult and requires sophisticated methods as well as care and experience. Often the numerical inaccuracy may be higher than the errors due to the LDA. For many defect studies an accuracy with errors below 0.1 eV for the relevant total-energy *differences* is needed even for a *qualitative* de-

scription as 0.1 eV is the typical order of magnitude for energy barriers and energy differences between atomic configurations. Therefore higher inaccuracies could give rise to a significantly different geometry and electronic structure.

An important deficiency of the present state of the theory concerns excitation properties, as, for example, optical absorption or emission. DFT-LDA is only designed for ground state properties. In order to handle excitations it is important to calculate the electron self energy (Sham and Kohn, 1966; Hedin and Lundqvist, 1969), which describes the modification of the exchange and correlation energy and the finite lifetime of the excitation (e.g., due to plasmon or electron–hole excitations). Furthermore, transition matrix elements can play an important role. A tractable and at the same time reliable approach for these purposes has not been developed so far. Therefore, only (semi) empirical calculations either neglecting the self-energy or taking a guessed ansatz (usually fitted to experiments) are used.

Localized defects in semiconductors present a particular challenge for the theory. Powerful methods and techniques to handle the ground state have been developed over the last 10 years, and more developments and improvements are underway. To date, no general theoretical approach exists that is suited for a reliable description of all possible defect candidates. In fact, a thorough investigation of point defects, including the local lattice distortions, is still a most demanding task. As a consequence, defect complexes (of more than two partners) and highly distorted transition-metal impurities have not been investigated in detail.

The calculation of the ground-state total energy and electron density, which are the key quantities of DFT-LDA, can be used to understand the electronic and atomic structure of defects. In addition, for temperature-dependent properties such as defect concentrations in thermodynamic equilibrium, it is possible to calculate thermodynamic potentials (the Gibbs free energy, for example) from the partition function of a canonical ensemble. Difficulties may arise because in many (maybe most) practical situations, thermodynamic equilibrium is not attained. For example, at or below room temperature, chemical reactions in the bulk may not be in equilibrium with the surface and with the crystal environment. Then it is often assumed that a "partial equilibrium" exists and that thermodynamics can be applied only to certain defect reactions. Such thermodynamic treatment has been done only recently by means of first-principle calculations (Scheffler, 1988; Biernacki and Scheffler, 1989; King-Smith *et al.*, 1989). For defects it was found (Scheffler, 1988; Biernacki *et al.*, 1989) that entropy differences of different defect configurations can reach values of about $3k_B$, where k_B is the Boltzmann constant. At $T = 1{,}000$ K, this entropy corresponds to 0.26 eV, which for many reactions may be of significant importance.

In this chapter we describe the basic concepts as well as the results of DFT-LDA calculations of *sp*-bonded defects in III/V zincblende-structure semiconductors. We mainly concentrate on structural and elastic properties and discuss the formation energies, stabilities, and defect reactions. Electronic levels and optical properties are discussed with less emphasis, because they are less reliable in the theory than the ground state electron density, the total energy, energy barriers, and forces (see Part III). We will assume throughout this chapter that the concentration of defects is low, so that their *statistics* is that of independent particles. Thus, when N_D is the number of defects and $2N_c = N_{III} + N_V$ the number of perfect crystal nuclei (cations and anions), the defect concentration is

$$[D] = \frac{N_D}{N_c} \ll 1. \tag{1}$$

This definition of the defect concentration will be used throughout this chapter. From [D] the number of defects per cubic centimeter is obtained by multiplying [D] by $4/\Omega$, where Ω is the volume in cubic centimeters of the conventional unit cell of the host crystal, which for a zincblende lattice contains four primitive unit cells. For GaAs, for example, we have $4/\Omega = 2.2 \cdot 10^{22}\ \mathrm{cm}^{-3}$. Most examples presented in this chapter are defects in GaAs. This is done because GaAs is the mostly studied material and because the *qualitative* properties of these examples and the conclusions are valid for other III/V compounds as well. Therefore, we feel that it is convenient to use GaAs practically as a synonym for a III/V compound and Ga and As as synonyms for a group-III crystal atom and a group-V crystal atom, respectively.

The remaining paper is organized as follows. In Part II we summarize the basic thermodynamic relations that are important for calculations of defect reactions and concentrations. In Part III we discuss some basic aspects of the density-functional theory and the local-density approximation for the exchange-correlation functional. We will not give a derivation of the theory because this can be found in the clearly written original papers (Hohenberg and Kohn, 1964; Kohn and Sham, 1965; Levy, 1982), as well as in greater detail in the books by Dreizler and Gross (1990) and Lundqvist and March (1983). We will present, however, a short description of the exchange-correlation interaction, and we will give some hints as to which cases require the LDA to be treated with special caution. Part IV then sketches the two main routes taken at present to evaluate defect properties: the self-consistent Green-function method and the supercell approach. Parts V–VIII describe results of recent calculations. We concentrate on *sp*-bonded defects, leaving out the first-row elements as well as transition-metal impurities. As men-

tioned earlier, special attention will be paid to formation energies, structural properties, and metastabilities. Part V summarizes calculations of the electronic structure and of the concentration of simple, intrinsic point defects in GaAs. Part VI gives a general description of antisite and antisite-like centers in GaAs and InP, and Part VII continues this discussion with respect to the *EL2* defect and its metastability. In Part VIII we discuss the properties of the substitutional donor Si in GaAs, which exhibits a shallow–deep structural transition, and we relate these results to experimental data of *DX* centers.

II. Thermodynamics of Defects in Semiconductors

1. Basic Concepts

The quantum mechanical system of a solid consisting of N_e electrons and N nuclei is described by the many-body Hamiltonian

$$H = H^{\mathrm{E}} + T^{\mathrm{I}}, \tag{2}$$

with

$$H^{\mathrm{E}} = T^{\mathrm{E}} + V^{\mathrm{E-I}}(\{\mathbf{r}_i\}, \{\mathbf{R}_I\}) + V^{\mathrm{E-E}}(\{\mathbf{r}_i\}) + V^{\mathrm{I-I}}(\{\mathbf{R}_I\}). \tag{3}$$

Here $\{\mathbf{r}_i\}$ denotes all position vectors of the electrons $(\mathbf{r}_1, \mathbf{r}_2, \ldots, \mathbf{r}_{N_e})$, and $\{\mathbf{R}_I\}$ denotes the positions vectors of all nuclei $(\mathbf{R}_1, \mathbf{R}_2, \ldots, \mathbf{R}_N)$. The kinetic energy operators of the electrons T^{E} and nuclei T^{I} are given by

$$T^{\mathrm{E}} = \sum_{i=1}^{N_e} -\frac{\hbar^2}{2m}\Delta_i \tag{4}$$

and

$$T^{\mathrm{I}} = \sum_{I=1}^{N} -\frac{\hbar^2}{2M_I}\Delta_I, \tag{5}$$

and the Coulomb repulsion of the electrons $V^{\mathrm{E-E}}$ and of the nuclei $V^{\mathrm{I-I}}$ is

$$V^{\mathrm{E-E}} = \frac{e^2}{8\pi\varepsilon_0} \sum_{\substack{i,j \\ i \neq j}}^{1 \cdots N_e} \frac{1}{|\mathbf{r}_i - \mathbf{r}_j|} \tag{6}$$

and

$$V^{I-I} = \frac{e^2}{8\pi\varepsilon_0} \sum_{\substack{I,J \\ I \neq J}}^{1\cdots N} \frac{Z_I Z_J}{|\mathbf{R}_I - \mathbf{R}_J|}, \tag{7}$$

where e is the electron charge, the charge of the Ith nucleus is $-Z_I e$, and ε_0 is the permittivity of free space. The attractive interaction between the electrons and the nuclei may be written in the form

$$V^{E-I} = \sum_{i=1}^{N_e} v(\mathbf{r}_i) \qquad \text{with} \qquad v(\mathbf{r}) = \sum_{I=1}^{N} V_I(\mathbf{r} - \mathbf{R}_I), \tag{8}$$

where V_I is the potential energy of an electron due to the nucleus I:

$$V_I(\mathbf{r} - \mathbf{R}_I) = -\frac{e^2}{4\pi\varepsilon_0} \frac{Z_I}{|\mathbf{r} - \mathbf{R}_I|}. \tag{9}$$

In many cases it may be advantageous to use the *frozen-core approximation*, in which the strongly bound electrons in closed shells are treated together with the nuclei as rigid ions. This approach often increases the numerical accuracy especially when applied together with the pseudopotential concept (see Section IV.7). In this case N_e is the number of valence electrons only and V_I in Eqs. (8) and (9) denotes the pseudopotential of the ion I.

The eigenvalue problem of the Hamiltonian H of Eq. (2) is solved by using the Born–Oppenheimer approximation. One then neglects the electron–phonon coupling, which implies that the states of the Hamiltonian of the electron system H^E of Eq. (3) are calculated separately in a first step by considering the coordinates of the nuclei as parameters. Using the density-functional theory, described in Section III.4, the lowest eigenvalue of H^E is calculated, which gives the ground-state total energy $E_0^{el}(\{\mathbf{R}_I\})$ as a function of the positions of the nuclei and which is called the Born–Oppenheimer total-energy surface. In the second step the vibrational energy spectrum is calculated at a certain point in configuration space, $\{\mathbf{R}_I^0\}$. Typically, $\{\mathbf{R}_I^0\}$ corresponds to the relevant minimum of the Born–Oppenheimer surface or is very close to it. $E_{0\mu}^{vib}(\{\mathbf{R}_I^0\})$ is then calculated as the eigenvalues of the vibrational Hamiltonian

$$H^{vib} = T^I(\{\mathbf{R}_I\}) + E_0^{el}(\{\mathbf{R}_I\}) - E_0^{el}(\{\mathbf{R}_I^0\}). \tag{10}$$

The eigenvalues of the Hamiltonian H of Eq. (2) are given by

$$E_{0\mu}(\{\mathbf{R}_I^0\}) = E_0^{el}(\{\mathbf{R}_I^0\}) + E_{0\mu}^{vib}(\{\mathbf{R}_I^0\}). \tag{11}$$

In order to apply this for the calculation of the Gibbs free energy of the solid, we may introduce the volume V as the volume occupied by the atoms at their positions $\{\mathbf{R}_I^0\}$. We use the canonical ensemble and write the partition function in the form

$$Z_1(T, V, \{\mathbf{R}_I^0\}) = D_{\text{deg}}^{\text{el}} \exp\left\{-\frac{E_0^{\text{el}}}{k_B T}\right\} \sum_\mu \exp\left\{-\frac{E_{0\mu}^{\text{vib}}}{k_B T}\right\}, \tag{12}$$

where we have neglected the summation over the excited electronic states. This is a reasonable approximation unless the difference between the lowest excited electronic energy and the ground-state energy is not large compared with $k_B T$. In Eq. (12) the volume dependence of Z_1 has been noted explicitly. The degeneracy $D_{\text{deg}}^{\text{el}}$ of the electronic ground-state energy E_0^{el} of the considered geometry is the spin degeneracy in case of any stable or metastable atomic configuration, and because of the Jahn–Teller theorem there is no orbital degeneracy, k_B is the Boltzmann constant, and T the temperature. The geometrical configurational degeneracy will be considered in Section II.2. To find the Helmholtz free energy and other properties of the thermodynamic equilibrium of the solid, we restrict the just-outlined theory to those atomic positions $\{\mathbf{R}_I^0\}$ that are close to the equilibrium values defining stable or metastable states.

The Helmholtz free energy of a crystal containing only one defect is then given by

$$F_1(T, V, \{\mathbf{R}_I^0\}) = -k_B T \ln Z_1(T, V, \{\mathbf{R}_I^0\}) = F^{\text{deg}} + F^{\text{el}} + F^{\text{vib}}, \tag{13}$$

with

$$F^{\text{deg}}(T, \{\mathbf{R}_I^0\}) = -k_B T \ln D_{\text{deg}}^{\text{el}} \tag{14}$$

$$F^{\text{el}}(V, \{\mathbf{R}_I^0\}) = E_0^{\text{el}}(V, \{\mathbf{R}_I^0\}) \tag{15}$$

and

$$\begin{aligned} F^{\text{vib}}(T, V, \{\mathbf{R}_I^0\}) &= -k_B T \ln \sum_\mu \exp\left\{-\frac{E_{0\mu}^{\text{vib}}}{k_B T}\right\} \\ &= \sum_i \left[\frac{\hbar\omega_i}{2} + k_B T \ln\left(1 - \exp\left\{-\frac{\hbar\omega_i}{k_B T}\right\}\right)\right]. \end{aligned} \tag{16}$$

Here $\omega_i(V, \{\mathbf{R}_I^0\})$ denote the vibrational frequencies of the solid in the quasi-

harmonic approximation,[1] which have to be summed up (Born and Huang, 1954). For a finite crystal with periodic boundary conditions there are $3N$ vibrational modes. From the Helmholtz free energy it is possible to derive the entropy S_1 and the pressure p by

$$S_1(T, V, \{\mathbf{R}_I^0\}) = -\left(\frac{\partial F_1}{\partial T}\right)_{V,\{\mathbf{R}_I^0\}} \tag{17}$$

and

$$p(T, V, \{\mathbf{R}_1^0\}) = -\left(\frac{\partial F_1}{\partial V}\right)_T. \tag{18}$$

Solving the equation of state Eq. (18) for the volume $V_1 = V_1(T, p, \{\mathbf{R}_I^0\})$, we can calculate the Gibbs free energy

$$G_1(T, p, \{\mathbf{R}_I^0\}) = F_1(T, V_1(T, p, \{\mathbf{R}_I^0\}), \{\mathbf{R}_I^0\}) + pV_1(T, p, \{\mathbf{R}_I^0\}). \tag{19}$$

Under the condition of given temperature T and pressure p, the equilibrium volume and the equilibrium positions of the nuclei are determined by

$$\left(\frac{\partial G_1}{\partial \mathbf{R}_I^0}\right)_{T,p} = 0. \tag{20}$$

2. Defect Concentration and Gibbs Free Energy of Defect Formation

We will now consider the thermodynamic quantities that describe a semiconductor crystal containing one type of N_D noninteracting defects. This implies that we neglect defect–defect interactions, for example by Coulomb interaction, long-range lattice relaxation, and others. Let the partition function Z_1 of Eq. (12) describe a crystal containing one defect only, and let αN_c be the number of equivalent positions of the defect with respect to translational and point symmetry of the perfect crystal. For a tetrahedral site, α is equal to one.[2] Then, for a crystal containing $N_D \ll \alpha N_c$ defects, the

[1] We use the term quasi-harmonic approximation because the described approach allows us to take into account that the dynamical matrix and thus also the frequencies ω_i vary with the atomic positions.

[2] For a group IV semiconductor α would be equal to two for a tetrahedral site, because both atoms per unit cell are identical.

partition function is given by

$$Z(T, V, N_D) = \binom{\alpha N_c}{N_D} [Z_1(T, V)]^{N_D}, \tag{21}$$

where the configurational degeneracy of the positions of the defects has been taken into account and Z_1 is given by Eq. (12). The Helmholtz free energy of such a crystal is then

$$F(T, V, N_D) = -k_B T \ln Z = -k_B T \ln \binom{\alpha N_c}{N_D} + N_D F_1. \tag{22}$$

Equations (13)–(19) also define the Gibbs free energy of the *perfect crystal* with $2N_c$ atoms. Note that the number of atoms of the crystal with the defect may be different from $2N_c$. To find the change of the Gibbs free energy due to the incorporation of one defect, it may be necessary to calculate the Gibbs free energy of some free atoms that enter or leave the crystal. A defect $D^{(l)}$ is formed by the exchange of atoms $A_1, A_2, \ldots$ and electrons e^- between a perfect crystal, which we denote by 0, and a reservoir. This is described by a chemical reaction of the form

$$D^{(l)} \rightleftharpoons 0 + \sum_i \nu_i A_i - l e^-, \tag{23}$$

where ν_i is the number of neutral atoms A_i involved in the reaction and l is the charge state of the defect. We now consider different charge states and treat differently charged defects as different defects. This also takes into account that differently charged defects typically have a different geometry. A special example of Eq. (23) is the formation of a l-charged substitutional atom X at a Ga site in GaAs. This is described by the reaction

$$X_{Ga}^{(l)} \rightleftharpoons 0 + X - Ga - l e^-. \tag{24}$$

The reaction Eq. (24) is understood in such a way that a substitutional defect $X_{Ga}^{(l)}$ is created inside a perfect crystal and that the atom X enters the defect region whereas the Ga atom leaves this region. The meaning of the words "enter" and "leave" will be specified later, when we describe the defect concentrations and chemical potentials.

The change of Gibbs free energy of the system due to the incorporation of N_D defects is then

$$G(T, p, N_D) - N_D\left[G^{pc} - \sum_i \nu_i G(A_i)\right] = -k_B T \ln \binom{\alpha N_c}{N_D} + N_D\left[(F_1 - F^{pc}) + p(V_1 - V^{pc}) - \sum_i \nu_i G(A_i)\right]. \tag{25}$$

It consists of a configurational part and contributions describing the defect-induced changes of Helmholtz free energy $F_1 - F^{pc}$, volume $V_1 - V^{pc}$, and atomic contributions. Here $G(A_i)$ denotes the ground state energy of the nucleus (or rigid ion) and the electrons of atom A_i. In case of thermodynamic equilibrium and assuming $1 \ll N_D$, the change of the Gibbs free energy due to the creation of one defect is

$$\mu(D) = \frac{\hat{c}}{\hat{c}N_D}\left[G(T, p, N_D) - N_D\left(G^{pc} + \sum_i \nu_i G(A_i)\right)\right] = -k_B T \ln\left(\frac{\alpha N_c}{N_D}\right) + \mu^0(D), \tag{26}$$

where we have used the approximation of Stirling. The so-called standard term $\mu^0(D)$ can be written in the form

$$\mu^0(D) = -k_B T \ln D_{deg}^{el} + E_0^{el}(V_1, \{\mathbf{R}_I^0\}) - E_0^{el,pc}(V^{pc}, \{\mathbf{R}_I^{pc}\}) + F^{vib}(T, V_1, \{\mathbf{R}_I^0\}) - F^{vib,pc}(T, V^{pc}, \{\mathbf{R}_I^{pc}\}) + p(V_1 - V^{pc}) - \sum_i \nu_i G(A_i), \tag{27}$$

where $\{\mathbf{R}_I^{pc}\}$ and $\{\mathbf{R}_I^0\}$ denote the equilibrium positions of the atoms of the perfect crystal and of the crystal containing one defect, respectively. We have assumed that the ground state of the perfect semiconductor crystal is non degenerate.

When the system is in thermodynamic equilibrium at a given temperature T and pressure p, the Gibbs free energy necessary to create a defect according to Eq. (23) must be equal to the change of energy due to the environment, and we have

$$\mu(D^{(l)}) = \sum_i \nu_i \mu(A_i) - lE_F, \tag{28}$$

where E_F is the Fermi energy and $\mu(A_i)$ denotes the chemical potential of the reservoir for atom A_i. The term "reservoir" implies that energies and entropies of the atoms do not depend on the defect concentration. In the same

sense the Fermi energy acts as a reservoir for electrons or holes, if the concentration of the defect is small compared to the background doping. From Eqs. (26) and (28) we then obtain the defect concentration

$$[\mathrm{D}^{(l)}] = \frac{N_{\mathrm{D}^{(l)}}}{N_c} = \alpha(\mathrm{D}^{(l)}) \exp\left\{ - \frac{\mu^0(\mathrm{D}^{(l)}) - \Sigma_i \nu_i \mu(\mathrm{A}_i) + lE_\mathrm{F}}{k_\mathrm{B} T} \right\}. \tag{29}$$

The numerator in the exponential is often called the Gibbs free energy of defect formation. We see that it depends on the reservoirs of the atoms and of the electrons.

For the preceding example of a Ga-site substitutional defect (see Eq. (24)), we obtain

$$[\mathrm{X}_{\mathrm{Ga}}^{(l)}] = \frac{N_{\mathrm{X}_{\mathrm{Ga}}^{(l)}}}{N_c} = \alpha(\mathrm{X}_{\mathrm{Ga}}^{(l)}) \exp\left\{ - \frac{\mu^0(\mathrm{X}_{\mathrm{Ga}}^{(l)}) - \mu(\mathrm{X}) + \mu(\mathrm{Ga}) + lE_\mathrm{F}}{k_\mathrm{B} T} \right\}. \tag{30}$$

Here $\mu^0(\mathrm{X}^{(l)})$ is given by Eq. (27), and the atomic chemical potentials $\mu(\mathrm{X})$ and $\mu(\mathrm{Ga})$ are determined by the chemical state in which the atoms X and Ga are bound in the initial or final state of the chemical reaction outside or at the surface of the crystal. Typically, $\mu(\mathrm{X})$ and $\mu(\mathrm{Ga})$ can be controlled by the environmental conditions (partial pressure). To give one example: Ga may end up in a Ga-metal crystal or it may, if the crystal is held in As_2 gas, form together with $\frac{1}{2}\mathrm{As}_2$ a new GaAs unit cell. These two extreme cases imply that the Ga chemical potential $\mu(\mathrm{Ga})$ can be modified over a range of 2 eV, which can have a significant effect on the defect concentration (see Eq. (30)).

We close this section with the remark that defects can also be formed without any atoms leaving or entering the crystal. In such cases neighboring or distant defect pairs are created (e.g., a Frenkel pair or an antisite–antisite pair) independent of reservoirs. The reactions are discussed in the next section.

3. DEFECT PAIRS AND THE LAW OF MASS ACTION

In Sections II.1 and II.2 we considered crystals containing one type of noninteracting defects only. This approach, however, can be used as well to determine the concentration of pairs of point defects and higher-order complexes. In this section we consider the chemical reactions between defects forming a defect–defect pair. If all possible defects are in thermodynamic equilibrium with the conditions determined by the crystal environment and by the crystal bulk and surface, then there is also thermodynamic equilibrium

with respect to all reactions of the defects with each other. However, often the full thermodynamic equilibrium may not be attained, because the temperature may be too low so that certain reactions are kinetically hindered; this implies that some of the defects are frozen in metastable configurations. Equilibrium thermodynamics may then still be applied, but should be restricted to only certain defect reactions. The resulting state is usually called a "partial equilibrium."

We now discuss defect–defect reactions, concentrating on the formation of defect pairs. Let us consider a reaction of a defect A with charge state i and a defect B with charge state j to produce a defect pair AB with charge state l:

$$\mathrm{AB}^{(l)} \rightleftharpoons \mathrm{A}^{(i)} + \mathrm{B}^{(j)} - (l-i-j)\mathrm{e}^{-}. \tag{31}$$

The corresponding law of mass action follows from Eq. (29) and reads

$$\frac{[\mathrm{AB}^{(l)}]}{[\mathrm{A}^{(i)}][\mathrm{B}^{(j)}]} = \frac{\alpha(\mathrm{AB}^{(l)})}{\alpha(\mathrm{A}^{(i)})\alpha(\mathrm{B}^{(j)})} \exp\left\{-\frac{\Delta\mu}{k_{\mathrm{B}}T}\right\}, \tag{32}$$

where the concentration $[\mathrm{A}^{(i)}]$ of a defect $\mathrm{A}^{(i)}$ is defined by Eq. (1) and α is the number of equivalent positions of the defect per primitive unit cell of the crystal. The Gibbs free energy of pair binding is

$$\Delta\mu = \mu^0(\mathrm{A}^{(i)}) + \mu^0(\mathrm{B}^{(j)}) - (l-i-j)E_{\mathrm{F}} - \mu^0(\mathrm{AB}^{(l)}), \tag{33}$$

where $\mu^0(\mathrm{A}^{(i)})$ and $\mu^0(\mathrm{B}^{(j)})$ are the standard terms of the Gibbs free energy of defect formation (see Eq. (27)). Again we assume that the Fermi energy is independent of the reaction. Note that the reaction energy $\Delta\mu$ is independent of the chemical potentials of the reservoirs $\mu(\mathrm{A}_i)$, since according to Eq. (31) no atoms leave or enter the crystal.

The chemical reaction Eq. (31) may also be used in the special case of the annihilation of two defects, which may occur if a Ga antisite approaches an As antisite or if a Ga interstitial approaches a Ga vacancy. The reverse of the last reaction is the formation of a distant (i.e., noninteracting) Frenkel pair, which for the cation in GaAs reads

$$\mathrm{V}_{\mathrm{Ga}}^{(j)} + \mathrm{Ga}_{\mathrm{i}}^{(l)} + (j+l)\mathrm{e}^{-} \rightleftharpoons 0. \tag{34}$$

Here i denotes a specific interstitial site. The law of mass action gives

$$[\mathrm{V}_{\mathrm{Ga}}^{(j)}][\mathrm{Ga}_{\mathrm{i}}^{(l)}] = \alpha(\mathrm{V}_{\mathrm{Ga}}^{(j)})\alpha(\mathrm{Ga}_{\mathrm{i}}^{(l)}) \exp\left\{-\frac{\mu^0(\mathrm{V}_{\mathrm{Ga}}^{(j)}) + \mu^0(\mathrm{Ga}_{\mathrm{i}}^{(l)}) + (j+l)E_{\mathrm{F}}}{k_{\mathrm{B}}T}\right\}. \tag{35}$$

In general, the concentration of Ga vacancies (and that of Ga interstitials) will depend also on other reactions involving these defects. However, if reaction (34) dominates or if there exists a partial equilibrium for this reaction, we have $[V_{Ga}^{(j)}] = [Ga_i^{(l)}]$, and the concentration of vacancies is determined by

$$[V_{Ga}^{(j)}] = \sqrt{\alpha(V_{Ga}^{(j)})\alpha(Ga_i^{(l)})}\exp\left\{-\frac{\mu^0(V_{Ga}^{(j)}) + \mu^0(Ga_i^{(l)}) + (l+j)E_F}{2k_BT}\right\}. \quad (36)$$

Note the factor 2 in the denominator of the exponential, which increases the vacancy concentration significantly. It is simply due to the fact that reaction (34) does not involve atomic reservoirs and that *two* defects are created simultaneously. Analogous equations to (34) and (36) hold for the simultaneous creation of a distant antisite pair, and for this case the law of mass action reads

$$[As_{Ga}^{(i)}][Ga_{As}^{(j)}] = \alpha(As_{Ga}^{(i)})\alpha(Ga_{As}^{(j)})\exp\left\{-\frac{\mu^0(As_{Ga}^{(i)}) + \mu^0(Ga_{As}^{(j)}) + (i+j)E_F}{k_BT}\right\}. \quad (37)$$

Further details for the defect reactions are discussed in Part V.

III. *Ab-Initio* Calculation of the Electronic Ground State and of Atomic Vibrations

4. DENSITY-FUNCTIONAL THEORY

Modern *ab-initio* calculations of ground-state properties of solids are typically based on the density-functional theory of Hohenberg, Kohn, and Sham (Hohenberg and Kohn, 1964; Kohn and Sham, 1965; Levy, 1982; Dreizler and Gross, 1990). The basic theorem states that the ground-state energy E_0^{el} of the many-electron Hamiltonian H^E (see Eq. (3)) is a functional of the electron density $n(\mathbf{r})$ and has its minimum at the exact ground-state electron density. The equations that follow are given for nonmagnetic systems, but the extension to spin polarization is straightforward. In fact, other extensions such as to relativistic effects, excited states, and time-dependent phenomena have also been discussed in the literature (see Dreizler and Gross, 1990, for more details). They are, however, not important to the problems addressed in this chapter. The variational property of the total-energy functional with respect to the electron density, together with the assumption that any physically meaningful electron density of the interacting many-electron problem can be represented by a density of noninteracting

fermions, leads to the Kohn–Sham equation (Kohn and Sham, 1965; Levy, 1982):

$$\left[-\frac{\hbar^2}{2m}\nabla^2 + v(\mathbf{r}) + v_{\mathrm{H}}(\mathbf{r}) + v_{\mathrm{xc}}(\mathbf{r}) \right] \psi_i(\mathbf{r}) = \epsilon_i \psi_i(\mathbf{r}). \tag{38}$$

The Hartree potential is given by

$$v_{\mathrm{H}}(\mathbf{r}) = \frac{e^2}{4\pi\varepsilon_0} \int \frac{n(\mathbf{r}')}{|\mathbf{r}-\mathbf{r}'|}\, d\tau', \tag{39}$$

and the exchange-correlation potential is defined by

$$v_{\mathrm{xc}}(\mathbf{r}) = \frac{\delta E_{\mathrm{xc}}[n]}{\delta n(\mathbf{r})}, \tag{40}$$

where $E_{\mathrm{xc}}[n]$ denotes the exchange and correlation functional. Equation (38) is a single-particle equation and can be solved by "standard techniques" (see Section IV). The electron density is given by the eigensolutions of the Kohn–Sham equation (38):

$$n(\mathbf{r}) = \sum_i n_i |\psi_i(\mathbf{r})|^2, \tag{41}$$

where n_i is the occupancy of the ith orbital. Typically n_i is one for states below E_{F} and zero otherwise. If defect levels coincide with the Fermi energy, fractional occupancy numbers of the highest occupied states are also possible. Since both potentials in Eqs. (39) and (40) are functionals of the electron density, the Kohn–Sham equation, together with Eq. (39)–(41), has to be solved self-consistently. The total energy is

$$E_0^{\mathrm{el}} = \sum_i n_i \left\langle \psi_i \left| \frac{-\hbar^2}{2m}\nabla^2 \right| \psi_i \right\rangle + \int [v(\mathbf{r}) + \tfrac{1}{2}v_{\mathrm{H}}(\mathbf{r})] n(\mathbf{r})\, d\tau + E_{\mathrm{xc}}[n] + \frac{e^2}{8\pi\varepsilon_0} \sum_{\substack{I,J \\ I\neq J}}^{1\cdots N} \frac{Z_I Z_J}{|\mathbf{R}_I^0 - \mathbf{R}_J^0|}. \tag{42}$$

This expression is in principle exact. However, in practice one approximation is necessary: Although $E_{\mathrm{xc}}[n]$ is a *universal* functional, i.e., there is only one functional that describes all systems, its general form is not known. In fact, it is not clear whether a simple, closed mathematical expression exists for $E_{\mathrm{xc}}[n]$. Only for the interacting many-electron system of constant electron

densities has the exchange-correlation energy per particle, $\epsilon_{xc}^{LDA}(n)$, been calculated by Ceperley and Alder (1980) using the quantum Monte Carlo method. The corresponding functional

$$E_{xc}^{LDA}[n] = \int n(\mathbf{r})\epsilon_{xc}^{LDA}(n(\mathbf{r}))d\tau \tag{43}$$

is called the local-density approximation of the exchange-correlation functional. It is exact for many-electron systems of constant density, but for inhomogeneous systems (where $\nabla n(\mathbf{r}) \neq 0$) it is of course an approximation. E_{xc} should describe all quantum-mechanical many-body effects: It should correct the self-interaction of the particle with itself, which is contained in the Hartree potential (see Eqs. (39) and (42)), it should take care of the Pauli principle, and it should describe the corrections that arise because the kinetic energy of noninteracting particles (the first term in Eq. (42)) neglects the Coulomb-interaction-induced correlation of the particle motion. The exchange and correlation functional $E_{xc}[n]$ may be written in the form

$$E_{xc}[n] = \frac{e^2}{8\pi\varepsilon_0}\int \frac{n(\mathbf{r})n_{xc}(\mathbf{r}, \mathbf{r}')}{|\mathbf{r}-\mathbf{r}'|}d\tau d\tau', \tag{44}$$

where $n_{xc}(\mathbf{r}, \mathbf{r}')$ is the density of the exchange-correlation hole

$$n_{xc}(\mathbf{r}, \mathbf{r}') = n(\mathbf{r}')(g(\mathbf{r}, \mathbf{r}')-1), \tag{45}$$

with

$$\int n_{xc}(\mathbf{r}, \mathbf{r}')d\tau' = -1 \tag{46}$$

and where $g(\mathbf{r}, \mathbf{r}') = g(\mathbf{r}', \mathbf{r})$ denotes the density–density pair correlation function. It can be shown that only the part of n_{xc} depending on $|\mathbf{r}-\mathbf{r}'|$ and $\mathbf{r}$ contributes to $E_{xc}[n]$. From these properties it follows that when $g(\mathbf{r}, \mathbf{r}')$ is replaced by g^{LDA}, part of the errors introduced by this approximation cancel when evaluating E_{xc} (Gunnarsson and Lundquist, 1976; Fahy *et al.*, 1990).

Almost all density-functional theory calculations performed so far have used the local-density approximation (Eq. (43)) or an approximation closely related to it. Experience has shown that this approach gives reliable total-energy surfaces, and thus structural, elastic, and vibrational properties are generally described remarkably well. For very inhomogeneous systems, as for example free atoms, the error due to the LDA can be quite significant (i.e., several electron volts). Consequently, calculated cohesive energies (i.e., the

difference of the total energy per atom of the crystal and of the free atom) can be wrong by about 1 eV (see, for example, Farid and Needs, 1992). It is generally believed that the error for energy *differences* of different geometries in solid-state systems (perfect crystals, surfaces and defects) is much lower. Experience supports this optimistic hope. The most severe problems of DFT-LDA calculations for solids reported so far concern magnetic systems. To be precise, this refers to the LSDA (local spin-density approximation). The calculations give a nonmagnetic fcc ground state of iron instead of the ferromagnetic bcc crystal (see Leung *et al.*, 1991, and references therein). Furthermore, the calculated $T \to 0$ ground states of metal oxides (e.g., the high-T_c superconductors) are nonmagnetic, whereas experiments show that they are ferromagnetic. We believe that these problems sound worse than they really are. It is important to note that the variational property of DFT holds for all ground states of different symmetry-group representations (including spin). However, the LDA may introduce different errors for each of them. Therefore it is to be expected that in systems with nearly degenerate ground states the ordering of these ground states can be wrong. To give an example, the calculated energy difference between the nonmagnetic fcc-Fe and the ferromagnetic bcc-Fe phase is $\leqslant 0.1$ eV per atom. Comparing this theoretical result with experimental data, we have to conclude that the LSDA inaccuracy is of the order of 0.1 eV. The iron example thus shows that a small *quantitative* error can produce an important *qualitative* change of the physical properties. This should be taken as a warning to be cautious in interpreting DFT-LDA results for cases where nearly degenerate ground states occur.

With respect to defects in III/V compounds, the most severe difficulty of the DFT-LDA approach concerns electronic properties, in particular the calculated band gaps of semiconductors. These band gaps of the DFT-LDA single-particle spectrum are usually much smaller than the experimental (optical) band gaps. In fact, the band topology (i.e., the gaps at Γ, L, and X) is also often wrong. The reason is that for the correct functional $\delta E_{xc}[n]/\delta n$ will have a discontinuity when the number of electrons is changed (Perdew and Levy, 1983; Sham and Schlüter, 1983), and this discontinuity is not described properly by the LDA functional. To calculate the band gap, the ground-state total energies for the N_e, the N_e-1 and the N_e+1 electron systems are needed. Although for perfect crystals the electron densities for the N_e, N_e-1, and N_e+1 systems are practically identical, the true exchange-correlation functional has to be sensitive to the differences. In particular, the quantum-mechanical many-body effects of the added electron (the N_e+1 state, which contains a conduction-band electron) differ significantly from the corresponding interactions in the N_e and N_e-1 states. Obviously, the correct description of these differences by a density functional requires a quite complicated functional form. DFT-LDA apparently is a good method for

systems with a given number of electrons, but it is too rough to describe the differences that occur when the number of electrons is changed and significantly different orbitals get populated.

State-of-the-art calculations of the band gap and related quantities therefore do not use the density-functional approach but calculate the self-energy $\Sigma(\mathbf{r}, \mathbf{r}', \omega)$ to first order in the screened Coulomb interaction (Hedin, 1965). In the actual calculations the Green function and the inverse dielectric function are evaluated from single-particle energies and wave-functions of DFT-LDA calculations (see Godby *et al.*, 1988, and Hybertsen and Louie, 1986). Thus, it is assumed that the quasiparticle and DFT-LDA wave function are very similar.

It is interesting to note that although the band gaps of DFT-LDA calculations are typically much too small, the hydrostatic deformation potentials (i.e., the derivative of the Γ, L, and X band gaps with pressure) are in close agreement with measured values; see, for example, Fiorentini (1992). Because defect levels are largely affected by band edges, in particular if these have a high density of states, a wrong band gap and gap topology can induce significant problems for defect calculations. In Section VIII we will come back to this point.

Deep defects in semiconductors may exist in different charge states. A precondition for this is that at least one *defect level* is in the band gap. Let us therefore define what we call a *defect level*. By this we mean the energy to *thermally* remove an electron from (or to add one to) a localized orbital. The donor level is

$$\varepsilon(+/0) = \mu^0(\mathrm{D}^{(0)}) - \mu^0(\mathrm{D}^{(+1)}), \tag{47}$$

which is the difference in the Gibbs free energy of a crystal containing one neutral defect $\mathrm{D}^{(0)}$ and a crystal containing one positive charged defect $\mathrm{D}^{(+1)}$. As can be seen from Eq. (27), $\varepsilon(+/0)$ follows from the differences of the ground-state total energy $E_0^{\mathrm{el}}(\{\mathbf{R}_l^0\})$, of the vibrational part of the Helmholtz free energy, and of the volume work. A corresponding definition holds for the acceptor level. If we neglect the vibrational and volume terms, we may use the Slater–Janak transition-state theorem (Slater, 1974; Janak, 1978). This gives

$$\varepsilon(+/0) = \epsilon(N_e - \tfrac{1}{2}) - E_{\mathrm{FC}}(+), \tag{48}$$

where $E_{\mathrm{FC}}(+)$ is the (positive) Franck–Condon shift, which is due to lattice relaxation as a consequence of the change of the charge of the defect. Here $\epsilon(N_e - \frac{1}{2})$ is the highest occupied single-particle eigenvalue of a self-consistent DFT calculation for a system with $N_e - \frac{1}{2}$ electrons, calculated at the equilibrium geometry of the N_e-electron system. Because of electron–electron interactions this eigenvalue differs (for localized orbitals) from that obtained

from calculations with N_e electrons. The difference,

$$\epsilon(N_e)-\epsilon(N_e-\tfrac{1}{2})=\tfrac{1}{2}U, \tag{49}$$

is positive, and for deep defects U is usually of the order of 0.3 eV. U is called the on-site Hubbard correlation energy. If the same defect orbital can also accept an electron, we get

$$\varepsilon(-/0) = -\epsilon(N_e+\tfrac{1}{2})+E_{FC}(-). \tag{50}$$

The transition-state eigenvalue $\varepsilon(N_e+\frac{1}{2})$ is calculated at the equilibrium geometry of the N_e-electron system. Often the values of the Franck–Condon shifts $E_{FC}(+)$ (Eq. (48)) and of $E_{FC}(-)$ (Eq. (50)) for different charge states are about the same, but this is not valid in general. For deep defects the Franck–Condon shift, which is a positive number, can be significant. As a consequence the level difference

$$\varepsilon(0/-)-\varepsilon(+/0)=U-(E_{FC}(-)-E_{FC}(+))=U_{eff} \tag{51}$$

can even become negative for deep defects. This is what is called a *negative U* system. As a result of $U_{eff}<0$, the acceptor level is below the donor level, which means that the N_e-electron system is not stable. Then, with increasing Fermi energy the system will go from the N_e-1 state directly to the N_e+1 state, thus capturing two electrons simultaneously. While the single-particle eigenvalues as well as the transition-state eigenvalues are subject to similar DFT-LDA problems as the band gap, we note that the calculated Franck–Condon shift, because this is an elastic energy, agrees with experimental results.

Equations (48) and (50) give the levels with respect to the energy zero of the calculation. However, usually donor levels are referred to the bottom of the conduction band and acceptor levels are referred to the top of the valence band. This requires us to redefine the levels by $\varepsilon^{donor}=\varepsilon_{CB}-\varepsilon(+/0)$ and $\varepsilon^{acceptor}=\varepsilon(0/-)-\varepsilon_{VB}$. For deep-level defects, the distinction between donors and acceptors is only of limited value. We will therefore not follow this description, but we will refer all levels to the top of the valence band which we take as our energy zero.

5. VIBRATIONS

Within the adiabatic approximation for the electrons, the dynamics of the nuclei is described by the Hamiltonian of Eq. (10), where E_0^{el} is the total energy of the ground state of the electronic Hamiltonian of Eq. (3).

In order to study the vibrational properties of the Hamiltonian of Eq. (10), it is usually sufficient to apply the quasi-harmonic approximation.[1] The vibrational frequencies ω_i are then determined by

$$\det(\mathbf{D} - \mathbf{M}\omega_i^2) = 0, \tag{52}$$

where $\mathbf{M}$ is the matrix of atomic masses and $\mathbf{D}$ is the dynamical matrix

$$\mathbf{D} = \left(\frac{\partial^2 E_0^{\mathrm{el}}}{\partial \mathbf{R}_I \partial \mathbf{R}_J} \right)_{\{\mathbf{R}_I^0\}}. \tag{53}$$

Here $\{\mathbf{R}_I^0\}$ are atomic positions at or close to the stable (or metastable) geometry. From $E_0^{\mathrm{el}}(\{\mathbf{R}_I^0\})$ and $\mathbf{D}(\{\mathbf{R}_I^0\})$ we obtain the Gibbs free energy (Eq. (19)), and the stable or metastable geometry at given pressure and temperature then follows from Eq. (20).

The dynamical-matrix elements may be obtained from many self-consistent total energy calculations performed in the neighborhood of the equilibrium geometry. Similarly, an *ab-initio* molecular dynamics calculation, using the approach of Car and Parrinello (1985), could be performed (Blöchl *et al.*, 1990). These two "direct approaches" require an enormous amount of computer power. Instead, Scheffler and Scherz (1986) and Biernacki *et al.* (1989) (see also Scheffler and Dabrowski, 1988; Biernacki and Scheffler, 1989) adopted a different approach using a semi-empirical valence-force model, the parameters of which (i.e., approximate equilibrium geometry and force constants) are calculated from first principles. Thus, the main purpose of the valence-force model was to obtain numerically accurate second derivatives of the total energy, which are needed for the dynamical matrix (Eq. (53)). An even more efficient and more accurate approach, which allows us to evaluate the dynamical matrix directly without the intermediate step of a valence-force model, would be the so-called perturbed density-functional theory of Baroni *et al.* (1987) and Gonze and Vigneron (1989) (see also Fleszar and Gonze, 1990).

In each of the previously mentioned examples it is necessary to calculate total energies as well as total-energy derivatives. If an appropriate basis set is used, the *in principle* exact Hellmann–Feynman theorem can be applied also in practice (Scheffler *et al.*, 1982, 1985) in order to calculate forces on the atoms. Either the forces then determine the motion of the particles (in a molecular dynamics study) (Car and Parrinello, 1985; Blöchl *et al.*, 1990), or the derivatives of the forces give the components of the dynamical matrix (Bachelet *et al.*, 1986; Scheffler and Scherz, 1986; Scheffler and Dabrowski, 1988; Biernacki *et al.*, 1989).

These different methods have been applied to calculate the vibrational entropy of the vacancy in silicon (see Eqs. (16) and (17)). All studies give a

result of about $3–4k_B$. For other defects no calculations exist, but it is generally believed that comparable values (between 1 and $5k_B$) would be obtained.

IV. Methods and Techniques

6. INTRODUCTION

The evaluation of Eqs. (38)–(42) requires complicated methods and techniques. This is in particular so for low-symmetry systems, as for example defects in crystals, where Bloch's theorem is not valid. Such methods and techniques have been developed only during the last years (see Bernholc *et al.*, 1978, 1980; Baraff and Schlüter, 1978, 1979, 1984; Scheffler, 1982; Scheffler *et al.*, 1982; Gunnarsson *et al.*, 1983; Car *et al.*, 1984, 1985; Bar-Yam and Joannopoulos, 1984; Beeler *et al.*, 1985a, 1985b, 1990; Bachelet *et al.*, 1986; Scheffler and Dabrowski, 1988; Scheffler, 1989; Overhof *et al.*, 1991). To date the applicability of these methods and techniques is still limited to special systems, and new ideas and improvements of the theory are still important.

Several controllable approximations are necessary in an actual first-principles calculation. If carefully applied, they will not significantly affect the results for $n(\mathbf{r})$ and $E_0^{el}(\{\mathbf{R}_I^0\})$, but they cause certain numerical inaccuracies. The most accurate method developed so far is the self-consistent pseudopotential Green-function method (Bernholc *et al.*, 1978; Baraff and Schlüter, 1978, 1979, 1984; Scheffler, 1982; Scheffler *et al.*, 1982 and 1985) which, if used together with first-principles, norm-conserving pseudopotentials (Hamann *et al.*, 1979; Kerker, 1980; Bachelet *et al.*, 1982; Gonze *et al.*, 1990, 1991), gives a reliable description of ground-state properties of *sp*-bonded systems. In the LMTO (linear muffin-tin orbital) Green-function method (Gunnarsson *et al.*, 1983; Beeler *et al.*, 1985a, 1985b, 1990; Overhof *et al.*, 1991), the approximation of spherical potentials is introduced. Because of the variational principle in DFT, this is usually not a severe approximation, but it does not allow the evaluation of defect-induced lattice distortions. Cluster methods suffer from more severe (sometimes uncontrollable) problems: They impose artificial boundary conditions to the wave-functions, and they localize the wave-functions and charge densities to the size of the cluster, which can cause a wrong description of covalent binding. The super-cell approach also suffers from these problems of cluster approximations, but the imposed artificial periodicity usually represents a far less severe approximation. Furthermore, with modern techniques it is now possible to take a cell size of more than 50 atoms. This enables us a systematic test of cell-size–induced inaccuracies. Because of the high complexity of first-principles methods, there is always a

risk that some aspects may be overlooked in the calculations. It is therefore good to know if two independent groups, hopefully using different techniques, arrived at the same theoretical results.

In Section IV.7, we give a short sketch of the pseudopotential concept. The alternative, i.e., the LMTO theory, is not discussed, because it has not been developed yet to the same level of applicability to treat total-energy surfaces and lattice distortions. We like to mention, however, that for defects in silicon the LMTO method has been applied to interesting problems of defect science (Beeler *et al.*, 1985a, b, 1990), and recently even hyperfine fields have been calculated by Overhof *et al.* (1991). For the future we expect further exciting developments.

In Section IV.8, we outline the supercell method, which represents a conceptually simple theoretical approach to calculate defect properties but which has its clear limitations. These are that the low defect concentration of the true crystal (typically $\leqslant 1:10^5$) is modeled by a concentration of $\geqslant 1:10^2$. This induces quite strong defect–defect interactions, which may complicate the physics that the investigation aims to understand.

The best, but more sophisticated, approach is the Green-function method. It describes the concentration limit where only one defect is present in the macroscopic crystal. Thus, no artificial defect–defect interactions are created. Without going into details, the basic ideas of the Green-function method are described in Section IV.9.

7. PSEUDOPOTENTIALS

Because of the localized nature of the atomic core electrons, these states do not contribute significantly to the chemical binding. It is therefore possible and convenient to introduce the frozen-core approximation in which the core electrons are treated together with the nucleus as a rigid spherically symmetric charge distribution. This implies the replacement of the potentials of the nuclei (Eq. (9)), which enter Eqs. (8) and (38), by potentials of the frozen-core ions, and of $E_{xc}[n]$ and $v_{xc}[n]$ by $E_{xc}[n_{val}+n_{core}^{atom}]$ and $v_{xc}[n_{val}+n_{core}^{atom}]$. Here n_{core}^{atom} is the core electron density of an atomic calculation, and density-functional theory is then applied tothe valence electrons, n_{val}, only.

The pseudopotential theory takes an additional step (see, for example, Cohen, 1985, and references therein) in that it also removes the oscillations of the valence-electron wave functions in the core region, which are caused by the orthogonality to the core states. This is achieved by modifying

$$V^{ion}(\mathbf{r}) = -\frac{e^2}{4\pi\varepsilon_0}\frac{Z}{r} + \frac{e^2}{4\pi\varepsilon_0}\int \frac{n_{core}^{atom}(\mathbf{r}')}{|\mathbf{r}-\mathbf{r}'|}\,d\tau' \tag{54}$$

in the region close to the nucleus in an appropriate way that does not affect the valence-electron wave functions in the chemically important regions but that makes them smooth in the core region. This approach therefore allows an accurate representation of the pseudopotentials in terms of quite simple and numerically advantageous basis sets, such as plane waves or Gaussians.

An important step in the development of pseudopotential theory was to realize the condition of norm-conservation (Hamann *et al.*, 1979; Kerker, 1980). It implies that ionic pseudopotentials, which are derived from free-atom calculations, give a correct description of the scattering properties not only at the energy of the atomic eigenstates, but also in a rather wide energy range around it. This is an important condition for using free-atom derived pseudopotentials (often called *ab-initio* pseudopotentials) in different chemical environments. One disadvantage implied by the norm-conservation is that these pseudopotentials become nonlocal operators: They act differently on states with different angular momentum quantum numbers. As a result, such calculations consume much more computer time than those with local pseudopotentials. This is, however, not a severe problem, in particular as nowadays separable *ab-initio* pseudopotentials are constructed (Kleinman and Bylander, 1982; Gonze *et al.*, 1990, 1991) that remove this disadvantage.

The *ab-initio* pseudopotential concept has been very successful in computational condensed-matter physics, and many new developments still appear (Blöchl, 1990; Vanderbilt, 1990) in order to achieve even smoother potentials, which make calculations more efficient.

8. SUPERCELL METHODS

Probably the most simple and still quite accurate *ab-initio* method to calculate defect properties in a parameter-free way is given by the supercell approach. This approach uses "standard" bandstructure methods of a perfect crystal, where Bloch's theorem holds. These may, for example, be the pseudopotential plane wave, or the LMTO method. The supercell is a large unit cell (typically between 16 and 128 atoms) that may represent the perfect crystal or contains one defect. Obviously, one thus describes a lattice of defects, maybe better termed an alloy than a dilute defect system. If the cell is small (say, 16 atoms) the defect–defect interaction can be quite significant. For example, a defect level in the crystal band gap can then become a defect band with a dispersion of more than 1 eV. This defect–defect interaction is an artifact of the method. Often it may not be important for defect geometries and local lattice distortions, but sometimes it may. Therefore, a careful analysis of results is most important, and different cell sizes ought to be investigated.

9. GREEN-FUNCTION METHODS

The best way to handle the difference with respect to the translational symmetry between the perfect crystal and a crystal containing a defect is the Green-function technique. In density-functional theory the Kohn–Sham operator (see Eq. (38)) can be written as a sum of the Kohn–Sham operator of the perfect crystal, h^0, and a potential ΔV induced by the defect $h = h^0 + \Delta V$. The Green operators $G^0 = (\varepsilon - h^0)^{-1}$ and $G = (\varepsilon - h)^{-1}$ are then related by the Dyson equation

$$G = (1 - G^0 \Delta V)^{-1} G^0. \tag{55}$$

Surveys of the defect Green-function method are given by Pantelides (1978), Scheffler (1982), and Schlüter (1987). There are two main reasons why this method has been used so extensively. First, the Green function of the perfect crystal, $G^0(\varepsilon)$, can be calculated taking advantage of Bloch's theorem and using standard band structure methods. Second, the Dyson equation (Eq. (55)), which gives the properties of the defect, can be calculated from small matrices if atomic-like orbitals are used as basis functions, which are localized at the defect and at a number of neighbors of the defect site.

V. Electronic Structures and Concentrations of Native Defects

Native or intrinsic defects are imperfections of the perfect crystal that do not involve impurity atoms and that are in fact unavoidable in principle. However, their concentration can be controlled by the temperature, pressure and by the environment (partial pressure) of the crystal. The growth of crystals under conditions of controlled non-stoichiometry leads to different native defect concentrations.

In this section we describe the electronic properties, as well as the formation energies, of vacancies, antisites, and self-interstitials. We restrict this discussion to tetrahedral geometries. Consequently, wave functions and energy levels are labeled according to the T_d point group. In the case of vacancies, the relaxation of the nearest neighbors with respect to their perfect crystal positions may change the symmetry of the defect. A possible change of this relaxation due to the change of the charge of the defect has been discussed in Section III.4. In the case of Ga and As interstitials in GaAs, we place the defects at the tetrahedral interstitial sites. These results are meant as a guideline. We like to emphasize, however, that we do not expect that these geometries correspond to the true stable positions of self-interstitials. In fact,

similarly to self-interstitials in silicon, we expect that a split-bonded geometry is likely to have a more favorable energy; the energy difference to the here-discussed T_d site may be as large as 1.5 to 2 eV.

10. ELECTRONIC STRUCTURE OF INTRINSIC DEFECTS

We start with a discussion of the cation and anion vacancy. These are important defects *per se*, but an understanding of their electronic structure is also important for substitutional impurities and antisites. A substitutional defect is formed by filling a vacancy with a defect atom. Qualitatively, the electronic structure of substitutional centers then results from the interaction of the atomic orbitals of the defect atom with the localized states of the vacancy.

If an atom is removed from its lattice site, there are four dangling orbitals (ϕ_1, ϕ_2, ϕ_3 and ϕ_4) of the nearest neighbors pointing towards the vacant site. These four orbitals will form a fully symmetric $(\phi_1+\phi_2+\phi_3+\phi_4)$ linear combination, which belongs to the a_1 representation of the T_d point group, and threefold degenerate linear combinations $(\phi_1-\phi_2-\phi_3+\phi_4)$, $(\phi_1+\phi_2-\phi_3-\phi_4)$, and $(-\phi_1+\phi_2-\phi_3+\phi_4)$ having t_2 symmetry. This t_2 level has higher energy than the a_1 level because the signs in the corresponding wave functions alternating give it a higher kinetic energy. Figures 1 and 2 show the single-particle energies and squared wave functions of the Ga and

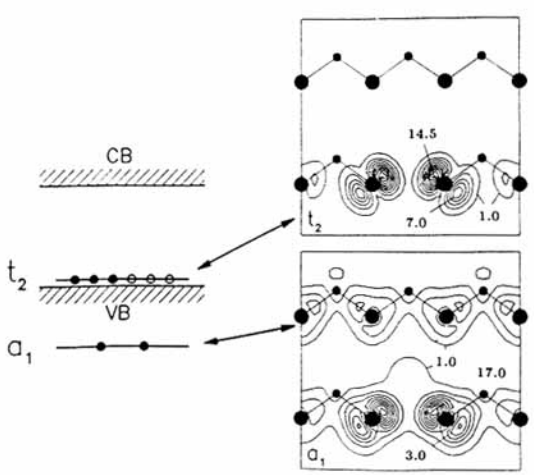

FIG. 1. Energy level diagram and contour plots of the two important states of the neutral Ga vacancy in GaAs. Displayed are the electron densities of the t_2 bound state (top) and the a_1 resonance (bottom) along the (110) crystal plane. Units are 10^{-3} bohr^{-3}.

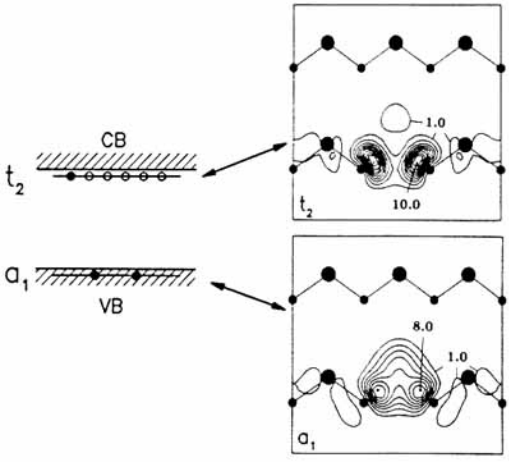

FIG. 2. Same as Fig. 1 but for the As vacancy in GaAs.

As vacancies in GaAs. In the case of the neutral cation vacancy there are three electrons missing, so that the t_2 level is occupied by three electrons (see Fig. 1). The corresponding energy level is close to the top of the valence band, and the calculations show that the Ga vacancy should be observable in the charge states $V_{Ga}^{(0)}$, $V_{Ga}^{(-)}$, $V_{Ga}^{(2-)}$, and $V_{Ga}^{(3-)}$, depending on the position of the Fermi level (Bachelet *et al.*, 1981; Baraff and Schlüter, 1985b; Laasonen *et al.*, 1992) and therefore acts as a triple acceptor.

The important orbitals of the As vacancy are shown in Fig. 2. For the neutral center five valence electrons have been removed together with the As core. As a consequence there is only one electron occupying the t_2 level, which is close to the bottom of the conduction band. The calculation shows that the tetrahedral As vacancy acts as a donor and is in the single positive charge state for all positions of the Fermi level. Recently Laasonen *et al.* (1992) found large lattice relaxations for the negatively charged defects $V_{As}^{(-)}$ and $V_{As}^{(2-)}$. Their calculations gave a 17% inward symmetry-conserving (breathing) relaxation, and a similar symmetry-breaking distortion for both charge states. This is in contrast to the rather small lattice relaxations calculated for the Ga vacancy and for $V_{As}^{(+)}$ and $V_{As}^{(0)}$ (Scheffler and Scherz, 1986; Laasonen *et al.*, 1992). The reason for the large Jahn–Teller distortion of $V_{As}^{(-)}$ and $V_{As}^{(2-)}$ is that when electrons are added to the neutral As vacancy, they form Ga–Ga bonds, thus reducing the symmetry so that the spatial-degenerate t_2 level is split, which leads to a lowering of the total energy.

Starting from the energy levels and wave functions of the Ga vacancy (see Fig. 1) and of an As atom, one can qualitatively understand the energy-level

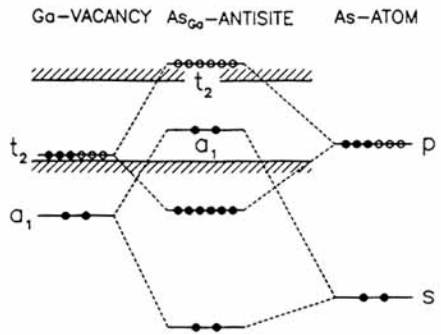

FIG. 3. Single-particle energies and interaction of a neutral cation vacancy in a III V compound (left) and a free anion atom (right) that result in an anion–antisite defect (middle).

structure of the As antisite As_{Ga}. Figure 3 shows how the splitting of the energy levels due to the interacting states leads to an a_1 state in the band gap. This state is occupied with two electrons for the neutral defect, and the As antisite thus is a double donor. The corresponding energy-level structures of the As vacancy and the neutral Ga antisite are shown in Fig. 4. Comparing this with Fig. 3 we see that the Ga_{As} levels are shifted to higher energies. This is because the energy levels of both the As vacancy and the free Ga atom are higher than the corresponding levels of the Ga vacancy and the free As atom. As a consequence, the Ga antisite has the antibonding a_1 level in the conduction band, whereas the bonding t_2 level is in the band gap. According to the calculations of Baraff and Schlüter (1985b), the Ga antisite acts as a double acceptor.

With respect to the physics depicted in Fig. 3, the single-particle eigenvalue $\varepsilon(a_1)$ of different antisite-like defects (e.g., P_{Ga}, As_{Ga}, and Sb_{Ga}) in GaAs

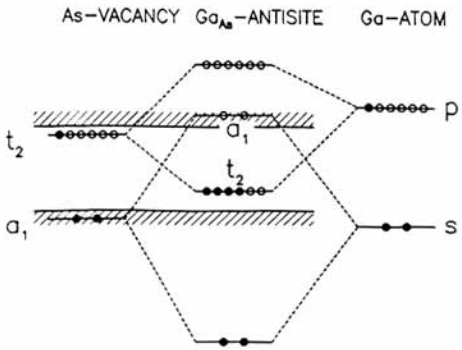

FIG. 4. Single-particle energies and interaction of a neutral anion vacancy in a III/V compound (left) and a free cation atom (right) that result in a cation–antisite defect (middle).

should, if lattice relaxation is neglected, follow the trend of the atomic *s*-orbital energy (Hjalmarson *et al.*, 1980). Since the donor transition involves a population change in this a_1 eigenvalue, we expect electronic levels to move with the atomic number of the group V defect atom towards higher energies (i.e., closer to the conduction band). This is indeed the trend found in calculations for *unrelaxed* tetrahedral antisites, i.e., when all host atoms remain at their perfect-crystal positions (see the $\varepsilon(+/0)$ results in parentheses in Table I).

When a substitutional defect is created, the neighboring atoms relax from their perfect crystal sites. Caldas *et al.* (1990) calculated the breathing relaxation of the neutral anion antisites, and their results are shown in Table I. It can be seen that the relaxation increases the anion–anion bond length (except for InP:$P_{In}^{(0)}$, which shows a small relaxation inwards; see ΔQ in Table I). The relaxation corresponds to a decrease of energies of the occupied a_1 donor levels and an increase of the optical excitation energy E_o, which corresponds to the excitation $a_1^2 t_2^0 \rightarrow a_1^1 t_2^1$; see Table I. Both effects are the

TABLE I

CALCULATED FRANCK–CONDON SHIFTS E_{FC}, DONOR LEVELS $\varepsilon(+/0)$ WITH RESPECT TO THE TOP OF THE VALENCE BAND, A CHARACTERISTIC OPTICAL EXCITATION ENERGY E_o, AND RELAXATION ENERGIES E_{rel} FOR DIFFERENT ANION–ANTISITE DEFECTS IN THE TETRAHEDRAL ATOMIC CONFIGURATION IN GaAs AND InP[a]

		E_{FC} (eV)	$\varepsilon(+0)$ (eV)	E_o (eV)	E_{rel} (eV)	ΔQ (Å)
	P	0.05	0.71	1.16	0.20	0.10
			(0.88)	(1.06)		
GaAs	As	0.03	0.81	0.97	0.42	0.12
			(1.05)	(0.91)		
	Sb	0.04	0.95	1.03	1.71	0.27
			(1.55)	(0.31)		
	P	0.10	0.95	1.50	0.01	−0.03
			(0.78)	(1.36)		
InP	As	0.09	1.3	1.32	0.00	0.01
			(1.2)	(1.20)		
	Sb	0.08	1.3	0.77	0.48	0.14
			(1.6)	(0.72)		

[a]Electronic levels $\varepsilon(+/0)$ defined by Eq. (47) are calculated from total-energy differences using two special **k** points. E_{rel} denotes the energy gained by the breathing relaxation of the first four atomic neighbors for the neutral defect, and ΔQ gives the distance each atom moves. Results in parentheses are obtained by keeping the atoms at perfect crystal positions.

largest for $Sb_{Ga}^{(0)}$, which also shows an increase of localization due to the relaxation (see the two lower contour plots in Fig. 5).

If one of the two a_1 electrons is removed, the bonds between the defect atom and its neighbors are strengthened because of the antibonding character of the deep-level wave function (see Fig. 5) and because the electrostatic interaction between the negatively charged neighbors (anions) and the positively charged antisite will attract the neighbors closer to the defect atom. The dependence of the relaxation of the four nearest neighbors on the charge state of the defect gives rise to moderate Franck–Condon shifts (E_{FC} in Table I). As expected from this discussion, the shifts are bigger for defects in more ionic InP than for defects in less ionic GaAs. It should be noted that the effect of long-range relaxation has not been considered in these calculations.

In contrast to the vacancies and antisites, very little is known about self-interstitials from the experimental point of view. Though interstitial point defects are certainly created by electron irradiation in similar amounts as vacancies, no isolated interstitials have been identified for far by EPR, DLTS, or other methods. A number of calculations for self-interstitials have been performed at the two positions of tetrahedral point symmetry: T_a, where the

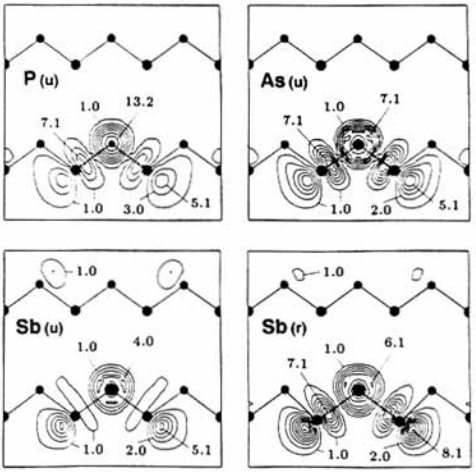

FIG. 5. Neutral anion–antisite-like defects in GaAs: Squared single-particle wave function of the filled a_1 state for the *unrelaxed* defects P_{Ga} [upper left panel labeled P(u)], As_{Ga} [upper right panel, As(u)], and Sb_{Ga} [lower left panel, Sb(u)], and for the relaxed Sb_{Ga} [lower right panel, Sb(r)]. We show the (110) plane. Contour lines are in units of 10^{-3} bohr^{-3}; the distance between the contour lines is 0.6 for P_{Ga} and 0.3 for As_{Ga} and Sb_{Ga}. (After Caldas *et al.*, 1990.)

defect atom has four anions as nearest neighbors, and T_c, where the defect atom has four cations as nearest neighbors. For both these tetrahedral positions we do not expect a strong covalent bond because the neighbor atoms are already bonded most favorably with the rest of the crystal. The valence orbitals of the interstitial atom indeed hybridize only weakly with the crystal states. They give rise to eigenfunctions of symmetry a_1 and t_2, the occupation of which depends on the position of the corresponding energy eigenvalues with respect to the Fermi energy. Results of self-consistent supercell calculations are shown in Fig. 6 for the As interstitial and in Fig. 7 for the Ga interstitial in the tetrahedral coordination. It is very probable that the As interstitials are unstable with respect to Jahn–Teller distortions and that the donor levels are then driven out of the gap when the As interstitial moves from the high-symmetry tetrahedral to a lower-symmetry equilibrium position. Similar distortions may also occur for the Ga interstitials, which may be the reason these defects have not been observed by EPR.

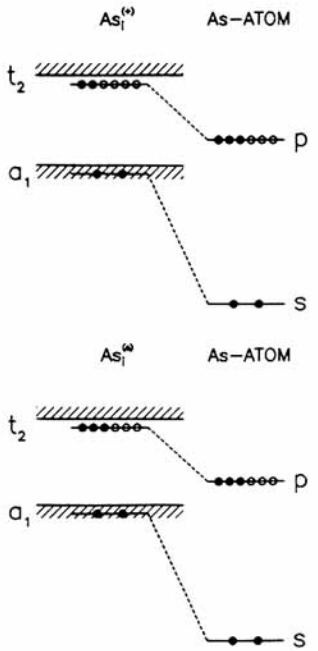

FIG. 6. Single-particle energies of the tetrahedral As-interstitials in GaAs. Top: at the T_a site (i.e., nearest neighbors are As) in the single positive charge state. Bottom: at the T_c site (i.e., nearest neighbors are Ga) in the neutral charge state.

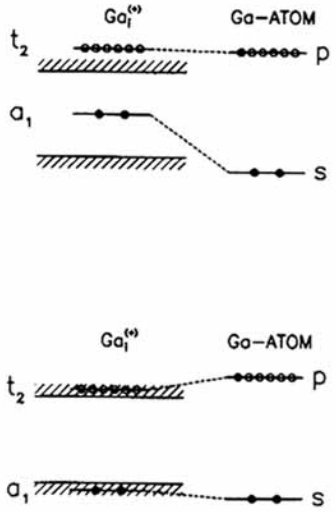

FIG. 7. Single-particle energies of the tetrahedral Ga-interstitials in GaAs. Top: at the T_a site (i.e., nearest neighbors are As) in the single positive charge state. Bottom: at the T_c site (i.e., nearest neighbors are Ga) in the single positive charge state.

11. NATIVE-DEFECT REACTIONS

In this section we consider all tetrahedral point defects of a GaAs crystal, which we denote by V_{Ga}, V_{As}, Ga_{As}, As_{Ga}, Ga_{T_a}, Ga_{T_c}, As_{T_a}, and As_{T_c}. In thermodynamic equilibrium the number of these defects is determined by Eq. (29). The formation energies of the defects (see the numerator of the exponential in Eq. (29)), which depend on the chemical potentials, and which directly determine the concentration of the defects, are shown in Fig. 8 for the

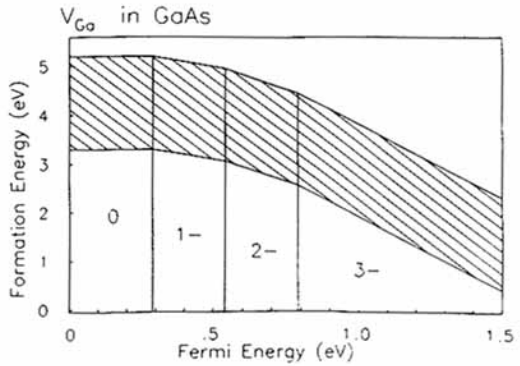

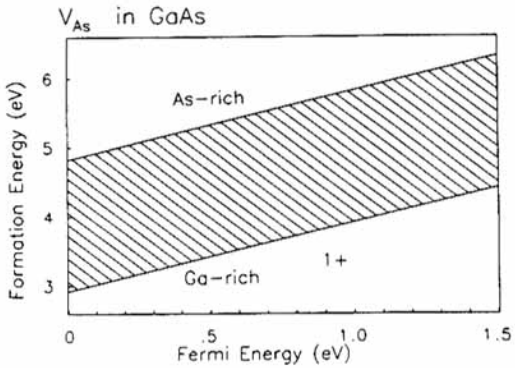

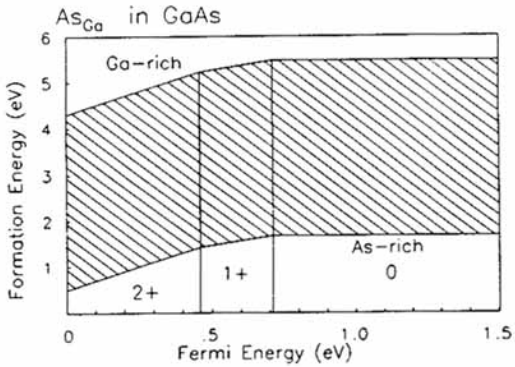

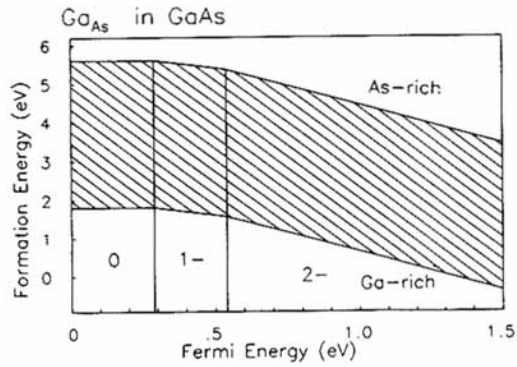

FIG. 8. Formation energies of the two vacancies (a, *b*) and the two antisites (c, d) in GaAs as a function of the Fermi energy E_F; see the numerator of Eq. (29). Shown are the two limiting cases for a crystal in an As-rich environment and in a Ga-rich environment (see text).

four substitutional native defects and in Fig. 9 for the interstitials. All these calculations (Heinemann and Scheffler, 1991) were performed using the supercell method with a 54-atom cell, a plane wave basis with $E_{cut} = 8$ Rydberg, and two special $\mathbf{k}$ points for the $\mathbf{k}$-integrations. Lattice relaxations have been neglected. They would lower the energies by 0.1–0.5 eV, if we restrict relaxations to the tetrahedral symmetry. The figures show how strongly the formation energy changes with the atomic and electron chemical potentials.

In order to describe the two extreme cases for the chemical environment, let us consider a GaAs crystal in thermodynamic equilibrium with an As_2 gas, which is the extreme As-rich condition (see Scheffler and Dabrowski, 1988). If the chemical potential of an isolated As atom is taken to be zero, the chemical potential of the As atom in an As_2 gas then is half the As_2 molecular binding energy. We therefore have $\mu(\text{As}) = -2.0$ eV. The chemical potential of Ga then is $\mu(\text{Ga}) = -4.8$ eV; this follows from the energy needed to remove one unit cell of GaAs (the cohesive energy), which equals 6.8 eV and a gain of 2.0 eV per As atom from the formation of As_2. These energies are approximate values of the corresponding Gibbs free energies which also include the entropy of the molecular gas and GaAs unit cells.

If, on the other hand, a GaAs crystal has droplets of Ga metal at the surface, the Ga chemical potential is given by the Ga-metal cohesive energy, which gives $\mu(\text{Ga}) = -2.8$ eV. The As chemical potential is then obtained from the energy needed to remove one GaAs unit cell, 6.8 eV, reduced by the Ga-metal cohesive energy to give $\mu(\text{As}) = -4.0$ eV. The cohesive energies are experimental values after Weast (1986).

From this discussion it follows that, depending on the partial pressure and chemical composition of the environment, the chemical potentials of the Ga and As atoms may be set within the ranges

$$\begin{aligned} -4.8 \text{ eV} &\leqslant \mu(\text{Ga}) \leqslant -2.8 \text{ eV}, \\ -2.0 \text{ eV} &\geqslant \mu(\text{As}) \geqslant -4.0 \text{ eV}, \end{aligned} \tag{56}$$

where the numbers on the left refer to the As-rich and the numbers on the right to the Ga-rich extreme conditions, as discussed. These two extreme cases for the chemical potentials, together with the calculated standard term μ^0 (see Eq. (27), give us two limiting cases for the defect formation energy according to the numerator of the exponential function of Eq. (29). The results for the eight intrinsic point defects in GaAs in tetrahedral coordination are shown in Figs. 8 and 9. Under the assumption that the defect concentration is not too large so that the defects can be treated as independent, these formation energies directly give the defect concentration (see Eq. (29)). It can be seen that the formation energies of the antisites are

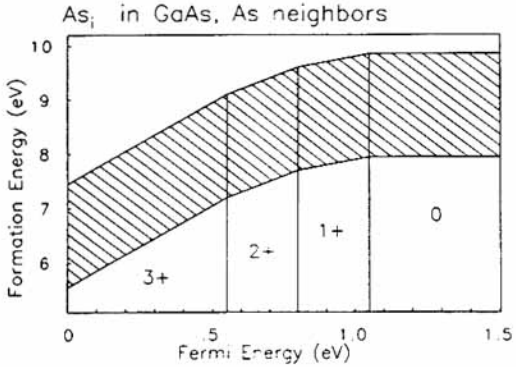

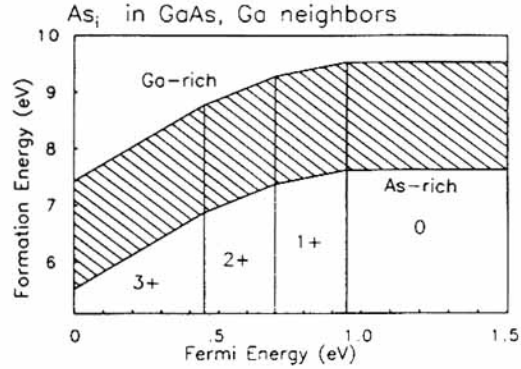

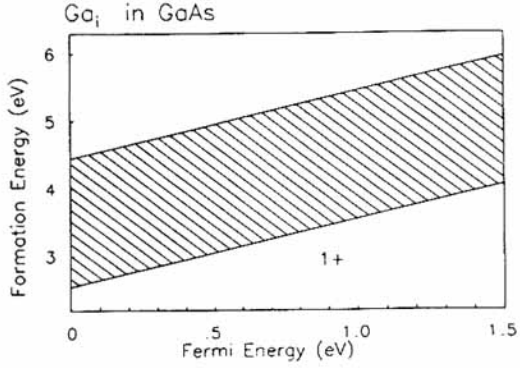

FIG. 9. Same as Fig. 8, but for the two As interstitials (a, b) and the two Ga interstitials (c) in GaAs in both tetrahedral sites T_a and T_c in GaAs.

more influenced by the environment (4 eV) than in the case of the vacancies or self-interstitials (2 eV).

The charge states of the defects were determined from the position of the corresponding transition states. For example, the transition state for the Ga vacancy was calculated to be $\varepsilon(0/-) = 0.29\,\text{eV}$ above the valence band. Therefore, the Ga vacancy is neutral when the Fermi energy is below that value and negatively charged when the Fermi energy is raised above that value.

Considering only the substitutional point defects of Fig. 8, we expect from these results that under As-rich conditions in *p*-type material, the As antisite is the dominating defect, whereas in *n*-type GaAs the formation energy of the Ga vacancy is lower than for the As antisite. The concentrations of the As vacancy and Ga antisite are much smaller in As-rich environment and at thermal equilibrium. Under Ga-rich conditions the results of Fig. 8 imply that the Ga antisites dominate over the As vacancies for all positions of the Fermi level, and the formation energies differ most for *n*-type material. It is interesting that for *n*-type material grown under Ga-rich conditions, there are more Ga vacancies than As vacancies. The reason for this is that in *n*-type material the Ga vacancy exists in the triple negative charge state, whereas the As vacancy is in the single positive charge state. Under Ga-rich conditions the As antisites are largely suppressed.

Concerning the interstitials (see Fig. 9), we find that their formation energies in GaAs for the two different tetrahedral interstitial sites are very similar because in both cases there are no covalent bonds formed and because the ionicity of GaAs is not large. The concentration of the As interstitials should be very small under all conditions. Although Fig. 9 shows only results for tetrahedral centers, we tend to conclude that isolated As interstitials will be also unfavorable in other geometries. We do not, however, rule out an important role for them in defect complexes. Ga interstitials may be present in GaAs in some relevant concentration, at least in *p*-type material. In fact, we find comparable concentrations of Ga interstitials and As vacancies under Ga-rich conditions for all positions of the Fermi level.

The point defects may also form bound defect pairs (see Baraff and Schlüter, 1986) and complexes of defects. Their concentrations can be calculated in the same way as for the point defects using Eq. (29). Obviously, the relative concentration of the bound pair and of the isolated defects is independent of the environment. It is given by the law of mass action, Eq. (32).

Native defects are related to a deviation from stoichiometry, and it is important to understand which of them dominates for given chemical potentials of the cations and anions outside the crystal. We describe the deviation from stoichiometry of a crystal $Ga_{1-x}As_x$ by

$$\delta = \frac{N_{Ga} - N_{As}}{N_{Ga} + N_{As}} = 1 - 2x. \tag{57}$$

It then follows

$$x = \frac{N_{As}}{N_{Ga} + N_{As}}, \tag{58}$$

where N_{Ga} and N_{As} are the numbers of cations and anions, respectively. For $x = \frac{1}{2}$, we have the perfect crystal stoichiometry. In the case of only small concentrations of the defects, and assuming that the crystal contains no impurities on lattice sites (that means that we disregard the doping here), the deviation from stoichiometry is approximately given by the sum over *all* possible types of native independent defects in their different charges states $D^{(i)}$ (see Eq. (29)):

$$\delta = \sum_{D^{(i)}} M_D[D^{(i)}] = \sum_{D^{(i)}} M_D \alpha(D^{(i)}) \exp\left\{-\frac{\mu^0(D^{(i)}) - \mu(D^{(i)})}{k_B T}\right\}, \tag{59}$$

where we have used Eqs. (28) and (29), and we have $M_D = -\frac{1}{2}$ for V_{Ga}, As_{T_c}, and As_{T_a}, $M_D = \frac{1}{2}$ for V_{As}, Ga_{T_c}, and Ga_{T_a}, $M_D = -1$ for As_{Ga}, and $M_D = 1$ for Ga_{As}. According to Eq. (29), the deviation from stoichiometry depends on the chemical potentials of the reservoirs of the atoms and electrons.

In practical cases a deviation from stoichiometry can be due to impurities and all different types of native defects, i.e., point defects, defect pairs, defect complexes, and other types of disorder such as precipitates that also depend on the history of the growing and annealing process. In order to find the dominating native point defects in thermodynamic equilibrium, which give the main contribution to Eq. (59), one has to consider the nine basic reactions between the native point defects (Kröger, 1964):

$$\begin{aligned}
V_{Ga}^{(i)} + V_{As}^{(j)} + GaAs + (i+j)e^- &\rightleftharpoons 0 \quad \text{(Schottky)} \\
As_{Ga}^{(i)} + Ga_{As}^{(j)} + (i+j)e^- &\rightleftharpoons 0 \quad \text{(antisite–antisite)} \\
Ga_T^{(i)} + As_T^{(j)} - GaAs + (i+j)e^- &\rightleftharpoons 0 \quad \text{(interstitial–interstitial)} \\
V_{Ga}^{(i)} + Ga_T^{(j)} + (i+j)e^- &\rightleftharpoons 0 \quad \text{(Frenkel)} \\
Ga_{As}^{(i)} + 2V_{Ga}^{(j)} + GaAs + (i+2j)e^- &\rightleftharpoons 0 \quad \text{(antisite–vacancy)} \\
Ga_{As}^{(i)} + 2As_T^{(j)} - GaAs + (i+2j)e^- &\rightleftharpoons 0 \quad \text{(antisite–interstitial).}
\end{aligned} \tag{60}$$

They have to be completed by interchanging Ga and As, and T can be one of the two interstitial sites T_c or T_a. The energies of all these reactions do not depend on the environment. They can be obtained from Figs. 8 and 9, taking for example the results for the As-rich case. We will only show a figure for one case, namely for the simultaneous creation of the two antisites, which is the

reverse of the second equation of Eq. (60). The reaction energy is given by

$$\Delta\mu = \mu^0(\mathrm{As}_{\mathrm{Ga}}^{(i)}) + \mu^0(\mathrm{Ga}_{\mathrm{As}}^{(j)}) + (i+j)E_{\mathrm{F}}, \tag{61}$$

and it is shown in Fig. 10. We see that the simultaneous creation of an As antisite and a Ga antisite is more likely in n-type GaAs than in crystals having the Fermi energy in the middle of the energy gap. Furthermore, we can use Fig. 10 in the following way: If, for example, the concentration of the As antisite and the reaction energy of Eq. (61) are known, then the law of mass action, Eq. (37), corresponding to the second reaction of Eq. (60) can be used to determine the concentration of the Ga antisite.

All other reactions can be obtained from linear combinations of the reactions of Eq. (60), and the reaction energies are determined similarly to Eq. (61) with the help of Figs. 8 and 9.

We close this section by emphasizing that a direct comparison of these theoretical results with experimental observations may often be difficult. This is largely because real crystals also contain defect complexes, precipitates, and dislocations. Furthermore, and in particular, we remind the reader that our discussion of defect concentrations relied on the assumption that the defects considered are present in low concentrations. Thus, defect–defect interactions should be negligible, and the Fermi level should be treatable as given by a reservoir determined by background doping and independent of the charge state and concentration of the considered defects. This is an idealization of growing and annealing processes in which the incorporation of donors and acceptors as well as the defect mobilities must also be taken

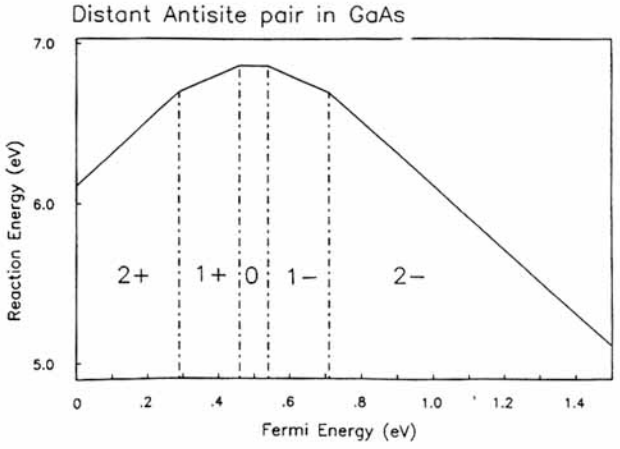

FIG. 10. Reaction energy of the simultaneous creation of an As antisite and a Ga antisite.

into account; see Wenzl *et al.* (1992). A number of models related to growth conditions, where the preceding assumptions are likely not to be valid, have been proposed to estimate the order of native defect concentrations from experimental data (see, for example, Sajovec *et al.*, 1990, and Wenzl *et al.*, 1990a, 1990b, 1991).

VI. An Intrinsic Metastability of Antisite and Antisite-like Defects

In the previous section we simply assumed that a defect is stable in one and only one local geometry. This assumption is appropriate for many situations. However, we had also seen that the nature of defects can be changed without changing the crystal stoichiometry (e.g., a Ga vacancy plus an As interstitial can be transformed into an As antisite). The controlling factor of the reactions noted in Eq. (60) and of their combinations was the "electron reservoir," i.e., the Fermi energy.

In this section we discuss an additional mechanism that changes the nature of a defect, where the changes are, however, due to a local atomic rearrangement. This is what is usually called a *defect metastability*.

Optically and thermally inducible structural transitions of defects have been known for several years (see, for example, van Kooten *et al.*, 1984; Chantre and Bois, 1985; Watkins, 1989; Caldas *et al.*, 1990). Because all up-to-date unambiguously identified metastable defects are complexes, where the metastability is understood in terms of a rearrangement of one of the constituents, it was interesting when in 1988 theoretical studies predicted (Chadi and Chang, 1988a; Dabrowski and Scheffler, 1988a, 1989a) a metastable behavior also for simple substitutional defects. Because no *direct* experimental proof of this predicted effect exists so far, it is understandable that this new type of metastability is not generally accepted. We believe, however, that the explanation of the general mechanism is well developed and that it is in fact quite plausible. We also note that significant indirect experimental evidence for this new effect exists.

In this part we describe the theoretically predicted properties of this new type of defect metastability. We show that it should play some role for antisite and antisite-like centers in practically all III/V compounds, and we explain the effect as a consequence of the capability of group V atoms to form sp^3 hybrids (tetrahedral geometry) as well as more or less pure p bonds like those in AsH_3. In Part VII we then concentrate on the As antisite in GaAs and relate the theoretical predictions to experimental data.

An anion antisite (or antisite-like defect) in a III/V compound is created when a group-V atom substitutes a group-III atom of the host. The

properties of these tetrahedrally symmetric defects were discussed in Section V, and it was explained that these centers give a deep bound state of the A_1 representation, and above it a state of the T_2 representation (see Figs. 3 and 5) that is usually within the conduction band.

Caldas *et al.* (1990) studied several anion antisite-like defects (P, As, and Sb) in GaAs and in InP. It was found that all these defects possess *in the neutral charge state* a metastable minimum in the total-energy surface, with the defect atom displaced along the [111] axis, roughly halfway between the substitutional site and the closest tetrahedral interstitial site (T_a). Figure 11 shows how the geometry and the valence electron density change upon moving the defect atom from the substitutional tetrahedral position to the displaced positions, which may be described as a vacancy-interstitial pair

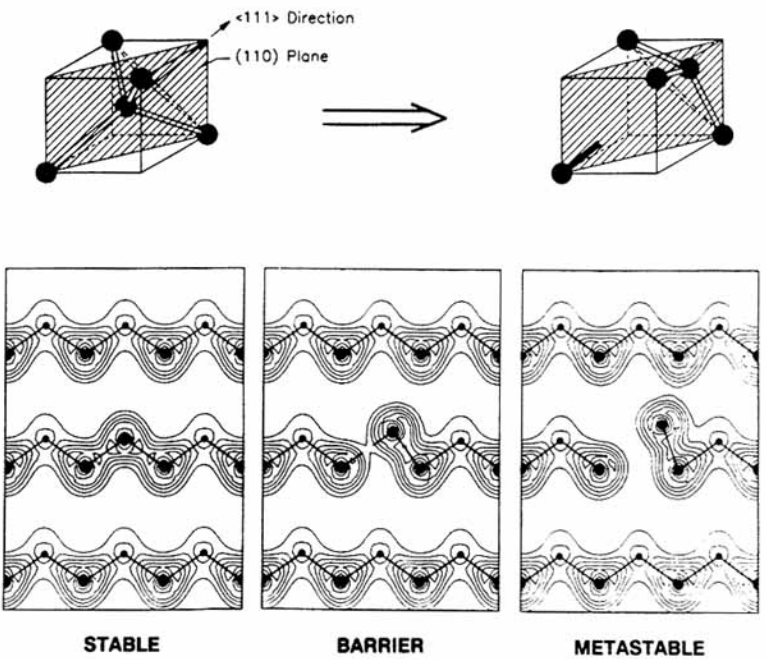

FIG. 11. Metastability of the As–antisite defect. Top: atomic structure. Bottom: the electron density in the (110) plane. Large circles represent As nuclei. Small circles represent Ga nuclei. The left-hand side shows the fundamental state, where the arsenic defect atom is bound to four nearest neighbors [only two are in the displayed (110) plane]. The middle panel shows the barrier region. The picture on the right-hand side corresponds to the metastable situation (the $V_{Ga}As_i$ defect pair). Here the arsenic defect is bound to three arsenic neighbors [only one of them is in the (110) plane]. The solid "dangling bond" in the top right-hand picture indicates the vacancy state, which is responsible for the barrier between the metastable and the fundamental configuration. (After Dabrowski and Scheffler, 1988b.)

(labeled V–I pair hereafter). We like to emphasize that the interstitial component of the pair should not be identified with the tetrahedral interstitial that was discussed in Section V: The tetrahedral interstitial position corresponds to nearly twice the displacement as that found in the calculations, and it would have a significantly higher total energy as well as a different electronic structure. In fact, the *qualitative* origin of the metastability is the capability of the defect atom to form a quadruple as well as a triple bond. The latter is not the case for a tetrahedral interstitial.

In Fig. 12 we show the corresponding electronic structure and the total-energy curves. The displacement of the antisite atom lowers the local symmetry to C_{3v}, and the single-particle t_2 state splits: $t_2(T_d) \rightarrow 2a_1(C_{3v}) + e(C_{3v})$. The single-particle $a_1(C_{3v})$ states of the displaced antisite with energies above the valence band are labeled $1a_1$ and $2a_1$. With respect to the many-electron wave functions, we note that the lowest-energy mean-field configurations of the A_1 representation are then $(1a_1^2 2a_1^0)$, $(1a_1^1 2a_1^1)$, and $(1a_1^0 2a_1^2)$, which may interact to yield three non-paramagnetic states ($S = 0$) that we label as $^1A_1$, $^1A_1^*$, and $^1A_1^{**}$. In Fig. 12a we depict the dependence of the total energies on the displacement Q of the defect atom for these three states. We also show in a schematic form the typical behavior of the single-particle eigenvalues (Fig. 12c). For small displacements Q, the energy of the ground state exhibits a parabolic behavior around the minimum at the

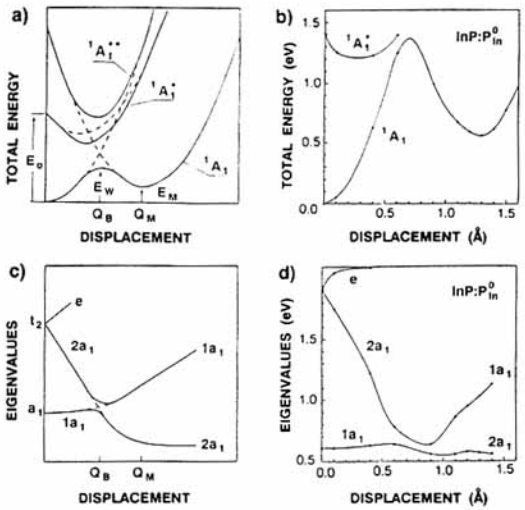

FIG. 12. Single-particle energies (bottom) and total energies for the ground and excited electronic configurations (top) as a function of the displacement of the defect atom along the [111] axis. Left: schematic description. Right: results of calculations for InP:P_{In}^0. (After Caldas *et al.*, 1990.)

substitutional site and is dominated by the configuration $(1a_1^2 2a_1^0)$. With larger displacement, the eigenvalue difference $\epsilon(2a_1)-\epsilon(1a_1)$ decreases, and the interaction between these two states as well as with other vacancy-like states increases. This results in a localization of the occupied a_1 state into a dangling bond at the crystal atom left behind, pointing into the direction of the evolving vacancy. In contrast, the wavefunction of the unoccupied a_1 state is localized at the displaced defect atom. Because the occupied vacancy-like a_1 state is antibonding with respect to the interstitial atom, the total energy of the system decreases with further increasing displacement of the interstitial until a metastable position is reached at Q_M. The usual way to picture this configuration interaction is shown in Fig. 12a, where to the right of Q_B the dominant configuration of the ground state is ascribed to the configuration $(1a_1^0 2a_1^2)$. Figures 12b and 12d show the results for the system $InP:P_{In}^{(0)}$.

In the calculations shown in Fig. 12b and 12d, the crystal atoms were kept at their perfect crystal positions. When the four neighbors of the defect are allowed to relax, only the details of the described picture change, but the qualitative behavior remains the same. The internal optical excitation energy E_o of the tetrahedral antisite (Fig. 12) is not much affected (see Table I in Part V), while the donor levels shift slightly to lower energy. The barrier height $E_B = E_W - E_M$ decreases (see Fig. 12 and Table II). An interesting result is that in the metastable configuration Q_M the donor levels of the six studied defects shift into the valence band.

The $GaAs:Sb_{Ga}$ center is particularly interesting because here the lattice relaxation results in *qualitative* changes of the defect properties. The unrelaxed Sb_{Ga} follows the chemical trends described in Section V, but it is an extreme case: At the substitutional site its a_1 single-particle eigenvalue is very high, the wave function of this state is quite delocalized (Fig. 5), and the optical excitation energy E_o is very small (Table I). The difference in size between the impurity (Sb) and the removed atom (Ga) makes the *V–I* geometry energetically more favorable than the substitutional geometry, i.e., $E_M < 0$ (Table II). However, after the lattice relaxes, the situation is changed. The most prominent changes occur in the substitutional configuration, where the Sb atom was squeezed between its four neighbors: These neighbors relax outwards by about 0.3 Å, which gives a gain of 1.7 eV. The a_1 wave function becomes more localized, and the $\varepsilon(+/0)$ electronic level shifts down in energy to 0.95 eV above the valence-band top. The calculated internal optical excitation energy E_o increases with the lattice relaxation to about 1 eV, which is a typical value for anion antisites in GaAs (Table I). Smaller changes are observed in the *V–I* configuration, where the system gains about 0.8 eV

TABLE II

CALCULATED BARRIER HEIGHTS E_W AND METASTABLE ENERGIES E_M FOR DIFFERENT ANION–ANTISITE DEFECTS IN THE VACANCY–INTERSTITIAL PAIR *V–I* ATOMIC CONFIGURATION IN GaAs AND InP[a]

		E_W (eV)	E_M (eV)	Q_M (Å)
GaAs	P	0.9	0.3	1.4
		(0.9)	(0.3)	(1.4)
	As	0.7	0.4	1.2
		(0.8)	(0.2)	(1.2)
	Sb	1.2	0.5	1.4
		(0.6)	(−0.4)	(1.6)
InP	P			
		(1.4)	(0.6)	(1.3)
	As			
		(1.2)	(0.5)	(1.4)
	Sb			
		(1.0)	(0.4)	(1.3)

[a] E_W is the barrier from the stable substitutional to the *V–I* configuration, E_M is the energy difference between the substitutional and *V–I* geometries, while Q_M gives the distance from the substitutional site to the *V–I* site (see Fig. 12a). Values in parentheses correspond to unrelaxed atomic positions. All results refer to neutral defects.

relaxation energy. Because of this difference in the relaxation energy in the substitutional and in the *V–I* geometries, the former becomes stable, while the latter is now metastable—as is the result found for the other anion antisites.

The discussed electronic structure (see Fig. 12) indicates the possibility of an optically inducible structural transition. If the system, initially at the T_d geometry ($Q = 0$ in Fig. 12), is excited from the ground state to the excited state $^1A_1^*$, it will lower its energy by a displacement of the defect atom in the [111] direction. For an observable structural transition the excited state $^1A_1^*$ at $Q = 0$ has to be above the local maximum of $^1A_1$ (at $Q = Q_B$, i.e., $E_o > E_W$). If this condition is fulfilled the defect will, with a certain probability, end up at the *V–I* configuration, where, if the temperature is low, it will be frozen in. For GaAs, Caldas *et al.* (1990) concluded from their calculations that the mentioned condition holds for the As and P antisites, while it does not for the Sb antisite. Hence, for Sb the transition is very unlikely (Bäumler *et al.*, 1989a, 1989b).

VII. The *EL2* Defect

12. INTRODUCTION

As a special example of the metastability discussed in Part VI we will now discuss the calculated properties of the As-antisite in GaAs. In particular we will relate these calculated properties of As_{Ga} to experimentally known properties of the famous *EL2* center in GaAs.

The *EL2* defect is the dominant deep donor in undoped GaAs crystals grown under As-rich conditions. Of particular interest is the physicochemical identification of *EL2* and the understanding of its unusual metastability: At low temperatures, illumination with white light (precisely $\hbar\omega \geqslant 1.18\,\text{eV}$) makes the deep *EL2* level disappear, and then the defect can be no longer detected (Martin, 1981; Martin and Makram-Ebeid, 1986), except under application of hydrostatic pressure Baj *et al.* (1991). Heating the sample to $T > 140\,\text{K}$ brings the defect and its deep level back in full concentration. Further details of this metastability are discussed in Chapter 2 of this book, and the most characteristic ones are summarized by Dabrowski and Scheffler 1989a. Most of the microscopic models for *EL2* that are discussed in the literature are complexes where the metastability is understood in terms of a rearrangement of one of the constituents. Because *EL2* is accepted as not being impurity-related (Martin and Makram-Ebeid, 1986; Weber and Omling, 1985), these models are built from native defects. The most often discussed models for *EL2* are aggregates of several As_{Ga} defects (Frank, 1986; Figielski and Wosinski, 1987), complexes of As_{Ga} with vacancies (Wagner and Van Vechten, 1987; Baraff and Schlüter, 1985a), and the distant As_{Ga}–As_i pair (von Bardeleben *et al.*, 1985, 1986; Bourgoin *et al.*, 1988; Meyer *et al.*, 1986, 1987; Meyer, 1988; Delerue *et al.*, 1987; Baraff and Schlüter, 1987; Baraff and Lannoo, 1988). In the last few years the distant As_{Ga}–As_i pair has attracted a particular attention. Von Bardeleben *et al.* (1985, 1986) proposed the pair on the basis of systematic thermal deep-level transient spectroscopy (DLTS) studies, which strongly indicated the existence of an As_i in the *EL2* formation process. This As_{Ga}–As_i pair model was strengthened by electron-nuclear double-resonance (ENDOR) studies by Meyer *et al.* (1986, 1987) and Meyer (1988), who concluded that the ENDOR data are due to a distant As_{Ga}–As_i pair, that the defect symmetry is C_{3v}, and that the As_i sits in the [111] direction directly coupling to the As_{Ga} at a separation of 4.88 Å. Theoretical work by Baraff and Schlüter (1987), Baraff and Lannoo (1988), and Caldas and Fazzio (1989) gave support for this As_{Ga}–As_i-pair model, and Delerue *et al.* (1987) explained the pair's metastable geometry in terms of a displaced As_i. All these theoretical studies were based on semiempirical, parametrized calculations.

Based on self-consistent total-energy calculations, Dabrowski and Scheffler (1988a, 1988b, 1989a and 1989b) questioned some details of the ENDOR

analysis. In particular, it was found that a distant pair of the type proposed by the ENDOR analysis is practically unbound. This makes it an unlikely candidate for the dominant defect in GaAs. Last but not least, it was pointed out that such a pair should have a shallow level close to the conduction band, which seems to be in conflict with what is presently known about the *EL2* center. It was pointed out, however, that the As_{Ga} may well pair with other centers and that an As_i may also be part of a complex. The position of the As_i would then be quite different to that assumed in the ENDOR analysis of Meyer *et al.* (1986, 1987). Whatever the nature of the complex including the As_{Ga} (and even leaving it open whether such a complex really exists), we believe that there is no indication that it affects the nature of the *EL2* metastability.

The symmetry of the *EL2* defect in the charge state, showing the characteristic *EL2* absorption and the interesting metastability, was directly investigated by absorption studies under uniaxial pressure. These experiments, by Kamińska *et al.* (1985), Kamińska (1987), Kuszko *et al.* (1986), Bergmann *et al.* (1988), Trautmann *et al.* (unpublished), and Nissen *et al.* (1900, 1991), give no indication of a complex defect, but show tetrahedral symmetry. Up to now, the suggestion of Kamińska *et al.* that *EL2* has tetrahedral symmetry and that it is identical to the isolated As_{Ga} antisite was not generally accepted (see, for example, Mochizuki and Ikoma, 1987; Levinson and Kefalas, 1987; Baraff *et al.*, 1988) because a simple Huang–Rhys picture together with the assumption that the defect couples only to a single-phonon mode was inconsistent with the experimental line shape (Martin and Makram-Ebeid, 1986), and because it was questioned that "optical absorption at the isolated antisite can produce the observed metastability" (see, for example, Baraff and Schlüter, 1987; von Bardeleben *et al.*, 1985, 1986; Krambrock *et al.*, 1992).

This short discussion shows the difficulty and active controversy about the *EL2* center, of which even the most basic property, namely its symmetry, is not generally agreed on.

13. THE TRANSITION TO THE METASTABLE CONFIGURATION

Chadi and Chang (1988a) and Dabrowski and Scheffler (1988a, 1989a) suggested independently that the *EL2* metastability is due to the $As_{Ga} \rightleftarrows V_{Ga} - As_i$ structural transition, which we already discussed in Section VI. For the neutral tetrahedral As_{Ga} we have an excited state $a_1^1 t_2^1$, which can be reached from the ground state by optical absorption. This state is orbitally degenerate, and as a consequence the system is unstable with respect to a symmetry lowering Jahn–Teller distortion. Dabrowski and Scheffler (1988a, 1989a) found the Jahn–Teller force for the [111] displacement to be about

twice as large as those for the [100] and [110] displacements. Thus, the Jahn–Teller effect will move the central atom in the [111] direction towards the nearest tetrahedral interstitial site. This lowers the symmetry of the defect to C_{3v} and results in a splitting of the $t_2(T_d)$ state (bottom of Fig. 12) into a lower $a_1(C_{3v})$ state and higher $e(C_{3v})$ state. Of these two, only the a_1 state is occupied (with one electron), which is the reason for the Jahn–Teller energy gain. In the C_{3v} point group, the electronic configuration of the excited state is now labeled as $1a_1^1 2a_1^1$ (see Part VI for the details of this notation).

Figure 13 displays the single-particle energies of the $1a_1$, $2a_1$, and e states (top), as well as the three total-energy curves obtained for the three electronic configurations $1a_1^2 2a_1^0$ (labeled F, which stands for fundamental), $1a_1^1 2a_1^1$ (labeled E, which stands for excited), and $1a_1^0 2a_1^2$ (labeled M, which stands for metastable). This figure should be taken in a semiquantitative way. It shows results of parameter-free calculations, but only one atom is moved, and all others are kept at their perfect-crystal positions. When this constraint is removed, the total energy decreases, but the general picture will not change.

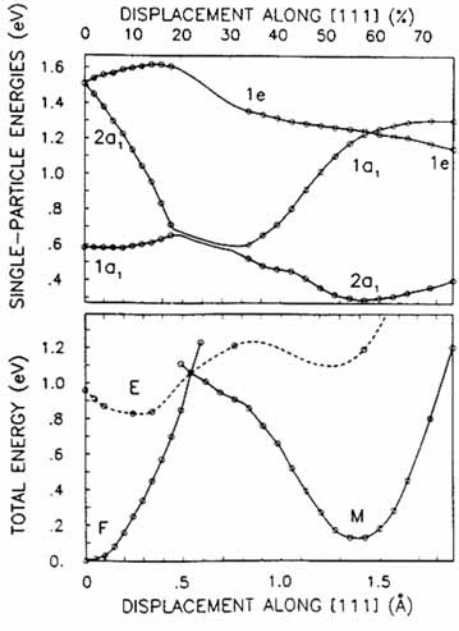

FIG. 13. Single-particle energies with respect to the valence band edge (top), and total energies of the $S = 0$ ground states (curves F and M) as functions of the position of the arsenic defect atom (bottom). Zero displacement refers to the tetrahedral As–antisite configuration. The total-energy curve labeled E is an electronic excited state with electronic configuration $1a_1^1 2a_1^1$. In these calculations all neighbors of the displaced arsenic atom were kept at their perfect-crystal positions (see text). (After Dabrowski and Scheffler, 1988a.)

The Jahn–Teller theorem predicts that the E total-energy decreases when the symmetry is reduced, i.e., when the As_{Ga} atom is displaced from its central position. This effect can be seen in the E total energy curve of Fig. 13, bottom. The geometry at the minimum of the E total energy curve may play a role in a non-Franck–Condon excitation, and Dabrowski and Scheffler (1988a, 1989a) therefore predicted a zero-phonon line at about 0.1–0.2 eV below the main peak (Fig. 13, bottom).

It is most likely that the excited system "falls back" from the E curve down to the F curve, the ground-state total energy. Then the system ends again as a tetrahedral As_{Ga} antisite. However, Fig. 13 shows that the $2a_1$ single-electron level decreases in energy very rapidly and therefore starts to mix with the $1a_1$ state. This allows for another electronic configuration, namely $1a_1^0 2a_1^2$. Thus, once excited to the E curve, the system has a certain probability of changing to the M curve. Then the arsenic defect atom will end a considerable distance (about 1.4 Å) from its initial central gallium site. We refer to this metastable atomic configuration as the gallium-vacancy–arsenic-interstitial pair, denoted by V–I. The As interstitial is about 1 Å away from the tetrahedral interstitial site. It is therefore chemically bound to only three arsenic atoms (Scheffler, 1989; Dabrowski and Scheffler, 1992). The transition to the metastable state competes with two other possible processes, namely the ionization of the excited state (where the excited electron of the As_{Ga} goes to the conduction band) and the deexcitation ($1a_1^1 2a_1^1 \rightarrow 1a_1^2 2a_1^0$) at smaller distortions. These two processes will bring the arsenic defect atom back to the fundamental configuration, i.e., to the tetrahedral As_{Ga} antisite. Because of these competitors it is obvious that the probability of the metastable transition is small and that it should be sensitive to local stress and other perturbations. It also depends sensitively on the conduction-band structure.

As the arsenic defect atom leaves the gallium site, its bond with one arsenic neighbor that is left behind is stretched, and it almost breaks when the defect enters the barrier region. This is shown in Fig. 11. The barrier of the structural transition is reached when the arsenic atom passes through the (111) plane of three As neighbors. In the metastable configuration, the arsenic defect atom (now an interstitial) binds to these three atoms (see Fig. 11), similarly to the bonding in crystalline grey arsenic. In the vacancy region there is one broken bond, which is filled with two electrons.

The electronic structure of the vacancy–interstitial pair found in the self-consistent calculations (top of Fig. 13 at 1.4 Å displacement) can be summarized qualitatively in terms of a simple tight-binding picture. The left- and right-hand parts of Fig. 14 show schematically the electronic structure of the isolated gallium vacancy and of an C_{3v}-site isolated arsenic interstitial. The vacancy with tetrahedral symmetry has a t_2 state close to the valence-band edge; in the neutral charge state this level (which can hold up to six

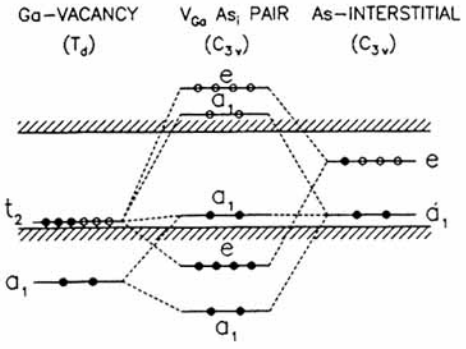

FIG. 14. Schematic summary of the electronic structure of the metastable configuration, i.e., of the $V_{Ga}^{(-)}As_i^{(+)}$ defect pair (middle), which can be understood in terms of a Ga vacancy (left) interacting with a C_{3v}-site As–interstitial (right). (After Dabrowski and Scheffler, 1988b.)

electrons) is filled with three electrons. Furthermore, the vacancy has an a_1-resonant state in the valence band. The arsenic interstitial at a C_{3v} symmetry site has an a_1 level in the lower and an e level in the upper half of the band gap. For the neutral interstitial, the a_1 state is filled with two electrons and the e state is filled with one electron. When the two systems interact (the middle part of Fig. 14), the $e(C_{3v})$ component of the vacancy $t_2(T_d)$ level and the interstitial $e(V_{3v})$ state form a bonding and an antibonding level that both disappear from the gap. The interaction of the t_2 and a_1 states of the vacancy with the interstitial a_1 states is slightly more complicated, but also follows qualitatively the tight-binding picture (see Fig. 14). The five electrons of the neutral gallium vacancy and the three electrons of the neutral arsenic interstitial will fill the three energetically lowest levels of the pair. From the wave-function character of the occupied states, we may label the pair $V_{Ga}^{(-)}As_i^{(+)}$. The self-consistent calculations of Dabrowski and Scheffler (1988a, 1989a) give the result that the empty a_1 and e states of the pair are close to the conduction-band edge, i.e., the corresponding acceptor levels should be degenerate with the conduction band. The highest filled state (labeled $2a_1$ in Fig. 13) is close to the valence-band edge, i.e., the corresponding electronic $\varepsilon(0/+)$ level should be degenerate or almost degenerate with the valence band; it has vacancy dangling-bond character and the wave-function is very localized. Also, the Green-function calculations by Ziegler *et al.* (1993) confirm this energy level structure showing that the acceptor levels are indeed close to the conduction band and that the $2a_1$ state is in the valence band. The constrained calculations of Dabrowski and Scheffler (1988a, 1989a), shown in Fig. 13, give a barrier for the neutral ground state of 0.92 eV between the minimum of the metastable configuration (the $V_{Ga}As_i$

pair) and the fundamental configuration (the As_{Ga} antisite). This value decreases to about 0.4 eV when the atoms of the cell are allowed to relax.

Figure 13 shows that the fourfold-coordinated As_{Ga} antisite and the metastable configuration with the threefold-coordinated As_i have very similar total energy. On the basis of the arguments presented, this result is indeed plausible for a group-V element. The origin of the barrier between the two configurations is, however, not immediately obvious. It may be understood by the fact that the covalent radius of an As atom is 1.2 Å. Therefore, the As_i is too "thick" to pass easily through the (111) plane of the three As atoms. This argument is, however, not complete and cannot explain why for other charge states the barrier will in fact disappear (see the next subsection). The main reason for the barrier is the filled vacancy-like dangling bond shown schematically in Fig. 11. This state is antibonding with respect to the arsenic interstitial, and its energy (the $2a_1$ level in Fig. 13) increases when the As interstitial is moved from the metastable configuration toward the vacancy. The occupied vacancy dangling orbital therefore contributes to the repulsion between the constituents of the metastable pair (Dabrowski and Scheffler, 1992). It is now clear that the barrier will change if one electron is removed from this level.

The ground-state total energy for the positively charged center with one electron at the Fermi level is given by

$$E^+ = E^0 + \varepsilon(+/0) - E_F. \tag{62}$$

E^0 is the neutral-charge-state total energy, i.e., the F and M curves of Fig. 13; $\varepsilon(+/0)$ is the transition state of the highest occupied single-particle level; and E_F is the Fermi level, to which the electron is transferred. Dabrowski and Scheffler (1988a, 1989a) obtained that the barrier is significantly reduced for the E^+ total energy, compared to E^0, namely by 0.4 eV. Thus, the barrier practically vanishes when one electron is removed from the vacancy-like dangling orbital of the $V_{Ga}As_i$ pair, which implies that a positive-charged As_{Ga} should not exhibit metastable behavior. This result suggests that a transition from the metastable V–I to the stable As_{Ga} configuration may be induced by a (temporary) hole capture at the V–I pair.

A second possibility of the $V_{Ga}As_i \rightarrow As_{Ga}$ regeneration is that an electron is (temporarily) captured in the $1a_1$ level of the metastable system. This corresponds to a temporary, negative charge state of the $V_{Ga}As_i$ pair. The total energy is given by

$$E^- = E^0 - \varepsilon(0/-) + E_F. \tag{63}$$

The transition-state energy $\varepsilon(0/-)$ is related to the occupation change in the

$1a_1$ state of the metastable configuration in Fig. 13. The calculations of Dabrowski and Scheffler (1988a, 1989a) predict that the E^- total-energy curve is very flat. Thus, the barrier is close to zero, but there are no strong forces pulling the As_i to the vacancy. Still, because the density of states at the bottom of the GaAs conduction band is very small, the negative charge state may live sufficiently long, and this electron-induced regeneration may be a likely regeneration channel.

14. Comparison of the Theoretical Results to the Experimental *EL2* Properties

A careful discussion of the *EL2* center requires us to take a variety of different properties into account. Dabrowski and Scheffler (1988a, 1989a) therefore compiled a detailed list of the most important "experimentally established properites of *EL2*" and compared these experimental properties with their theoretical results of the $As_{Ga} \rightleftharpoons V_{Ga}As_i$ defect. We will not repeat this detailed discussion here but refer the interested reader to the original publication. We just summarize that the comparison of the theoretical results for the isolated arsenic antisite and the $As_{Ga} \rightleftharpoons V_{Ga}As_i$ metastability (see Section VII.13) to the list of measured properties of the *EL2* defect reveals clear similarities. Both defects have basically the same electronic structure: They are double donors and give rise to two deep levels in the forbidden gap. Both defects are not paramagnetic when in the neutral charge state, show the midgap level, exhibit the metastability, and do not have a level in the upper part of the gap. In addition, both centers have the same pressure dependence of the transition state in the stable state (Ziegler and Scherz, 1992). The internal excitation of both centers is practically identical; the theoretical value of the Franck–Condon transitions at an As_{Ga} of 0.97 eV agrees well (within the expected accuracy of a parameter-free DFT-LDA calculation) with the *EL2* absorption main peak at 1.18 eV. The zero-phonon line in the experiments (0.14 eV below the main peak) may be compared to the theoretical result of 0.13 eV. However, we note that it is not yet clear if the experimental zero-phonon line is indeed a transition to the [111]-displaced arsenic defect atom.

As discussed in Section VII.13, optical excitation of the As_{Ga} can induce a structural transition via the intermediate total-energy curve labeled *E* in Fig. 13. The mechanism implies that the probability of this bleaching effect should be sensitive to the quality of the crystal. This is indeed known experimentally. For the positive charge state of the As_{Ga} antisite, in particular, theory and experiment tell that this is not quenchable directly, but only after the $As_{Ga}^{(+)}$ is transformed to an $As_{Ga}^{(0)}$. The theoretical barrier height for thermal recovery (i.e., for the $V_{Ga}As_i \rightarrow As_{Ga}$ transition), calculated as 0.4 eV, is close to the

experimental value of 0.34 eV. Also, the regeneration conditions are the same in the calculations and in experiments with *EL2*: There is a purely thermal process and an electron-induced ("Auger-like") regeneration process. The electron-induced deexcitation of *EL2* can be understood in the just-discussed theory in the following way: It starts with a thermally activated capture of a conduction-band electron in the $1a_1$ resonant state of the $V_{Ga}As_i$ pair. This capture is then followed by relaxation in the As_i to the fundamental configuration, where the captured electron is released. The third channel of regeneration of the fundamental atomic configuration, namely the hole-induced deexcitation, is expected to have a very small cross-section (Dabrowski and Scheffler, 1988a, 1989a). Indeed, such a process has not yet been observed for *EL2*.

Combined EPR-DLTS studies of von Bardeleben *et al.* (1986) indicated that *EL2* is destroyed if the sample is heated to 850°C and rapidly cooled afterwards, but it can be regenerated by 130°C annealing. This result can be qualitatively explained as follows: At high temperatures the $As_{Ga} \rightleftharpoons V_{Ga}As_i$ system dissociates into a gallium vacancy and an arsenic interstitial. Rapid cooling hinders the reverse process, and additional annealing at intermediate temperatures would be necessary to allow for the diffusion of the As_i and the association reaction $V_{Ga} + As_i \rightarrow As_{Ga}$. Again, as in many *EL2*-related experiments, the results of von Bardeleben *et al.* (1986) have not been fully reproduced by other researchers. Lagowski *et al.* (1986) and Lagowski (private communication) report different temperatures, namely 1,050°C (instead of 850°C) and 850°C (instead of 130°C). This demonstrates the high complexity of *EL2* investigations: Experimental results seem to depend strongly on the sample and on the crystal environment. For a more general discussion of how the crystal Fermi level (i.e., the electron chemical potential) and the gas in the crystal environment (the atomic chemical potential) can influence defect reactions and formation energies, we refer to Section II.3 and Part V.

The just-described calculations show that the neutral arsenic antisite exhibits, under optical excitation, an intrinsic metastability. The metastable transition is started by a Jahn–Teller effect, as speculated earlier by Scheffler *et al.* (1984) and Bachelet and Scheffler (1985). The good agreement between the calculated barrier (0.4 eV) and the experimental barrier suggests that the As_{Ga} antisite and *EL2* are identical defects. However, the uncertainty in the calculations was estimated as ± 0.2 eV. Therefore, we cannot positively rule out the possibility that another nearby (but weakly interacting) defect is in fact necessary to adjust the energy barrier to the 0.34 eV observed for *EL2*. Nevertheless, based on a detailed comparison with many experimental properties, we identify the basic mechanism of the *EL2* metastability as that of the As_{Ga} antisite.

VIII. The *DX* Centers

15. INTRODUCTION

In this part we discuss again a defect metastability of the type described in Part VI. In particular we consider the Si donor in GaAs. Although the basic mechanism (i.e., the $sp^3 \rightleftharpoons sp^2$ bonding and the nature of the barrier) is the same as before, some interesting additional aspects are identified. From a comparison with experimental results we relate these theoretical findings to experimental results of *DX* centers.

Substitutional group-IV Ga-site and group-VI As-site impurities in $Ga_{1-x}Al_xAs$ with low Al concentration ($x < 0.22$) are shallow donors. However, when x exceeds 0.22, or when the sample is put under high hydrostatic pressure, or when the sample is heavily doped, these defects are modified and become deep centers. Then they are called *DX* centers. For basic research the most exciting properties of *DX* centers are related to this pressure (or composition, or Fermi-level) inducible transition.

Similarly to the discussion on the identification and explanation of *EL*2 presented in the previous part, for *DX* there is also no general consensus about its microscopic structure and its metastability mechanism. However, correspondingly with the previous part, we will argue that the metastability is due to a structural change between the tetrahedral donor geometry and a vacancy–interstitial pair geometry (compare Part VI).

16. THEORETICAL RESULTS FOR THE Si DONOR IN GaAs UNDER PRESSURE

In this section we summarize results of density-functional–theory calculations of Dabrowski and Scheffler (1992). The main approximations in these studies were to replace the **k**-summation of the 54-atom super-cell by the Γ point and to neglect lattice relaxations. Unfortunately the theoretical results are now more sensitive to these approximations than was found for the defects discussed in Parts VI and VII. This is largely because *DX* centers exhibit a shallow $\rightarrow$ deep transition and because the results are more sensitive to the details of the conduction band. Tests had been performed also for other **k**-point sets and for some relaxed geometries, so that it was possible to roughly estimate how an improved calculation would modify the results. In order to investigate the pressure dependence, calculations were performed for different lattice constants. To ease the comparison with experimental results, Dabrowski and Scheffler (1992) decided to adjust the theoretical pressure scale by adding to their direct theoretical result a constant value of 31 kbar so that the Γ–X crossing occurs at the experimentally observed pressure. In Fig.

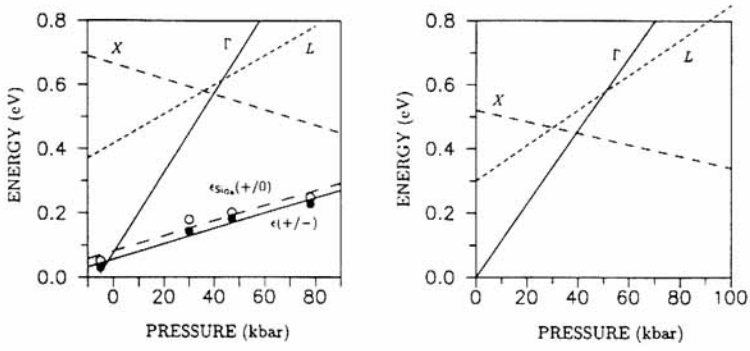

FIG. 15. Calculated (Dabrowski and Scheffler, 1992) (left) and measured (Lang *et al.*, 1979; Landoldt-Börnstein, 1982) (right) pressure dependencies of the GaAs conduction band minima, of the *DX* level, labeled as $\varepsilon(+/-)$ [full dots and solid line], and of the deep level of the tetrahedral Si_{Ga}, labeled as $\varepsilon_{Si_{Ga}}(+/0)$ [open dots and dashed line]. The zero of the theoretical pressure scale is adjusted such that the Γ–X crossing point is at 40 kbar. For the calculated defect levels lattice relaxation is neglected. We also note that the defect levels suffer from the Γ-point approximation of the **k** summation. Improving on this it was estimated that the $\varepsilon(+/-)$ line would shift up by about 0.3 eV and the $\varepsilon_{Si_{Ga}}(+/0)$ line would shift up by about 0.4 eV.

15 we show their results for the conduction band edges and for two Si defect levels, which we will discuss in more detail later. The pressure dependencies of the conduction band are reproduced very well by the theory, but the absolute gaps are too small, which is a typical result for converged DFT-LDA calculations (compare Section III.4).

In Fig. 16 we show the calculated total-energy curves for GaAs:Si, with the Si impurity atom displaced in the same way as the other impurities in Figs. 11, 12, and 13. The results of Fig. 16 were obtained with the host atoms frozen at their perfect crystal positions. Lattice relaxations lower the energies, but this does not affect any of the following conclusions. At first we discuss the curve corresponding to the negatively charged defect labeled $[D^{(-)}-e^{-}(E_F)]$, where the electron is at the Fermi level. We see in Fig. 16 that the minimum of this curve is at a displaced configuration, where the defect symmetry is C_{3v}. Here the defect should be called a vacancy–interstitial (*V–I*) pair. As in Parts VI and VII above, we emphasize that the Si-interstitial is not at the tetrahedral interstitial site of the lattice but closer to three As atoms. The bonding with these As atoms can be described as largely sp^2-like. We note that only for the negatively charged Si defect the *V–I* pair geometry has a lower energy than the substitutional, tetrahedral geometry. The mechanism that keeps the impurity at the interstitial site is essentially due to the highest occupied state of the defect. For the *V–I* pair, this state is a single As dangling orbital, indicated in the geometry-plot of Fig. 11 (top right) by the thick black line. It interacts only weakly with the Si interstitial. When the Si atom is

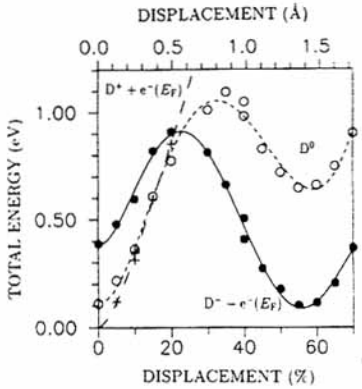

FIG. 16. Calculated total energy for GaAs:Si as a function of the Si position (Dabrowski and Scheffler, 1992). Zero displacement corresponds to the tetrahedral Si_{Ga} defect. 100% displacement would correspond to the nearest tetrahedral interstitial position, which would be the corner of the cube shown in Fig. 11. Three different charge states are shown. The Fermi level is taken at the minimum of the conduction band, which is at Γ. The lattice constant underlying these calculations is $a = 5.68$ Å, which corresponds to a pressure of -5 kbar in Fig. 15. The main approximations that may affect some quantitative results are the neglect of lattice relaxations and the replacement of the **k** summation by the Γ-point.

pushed towards the vacant site, this orbital, as well as the Si-centered orbitals, is compressed, which increases the electron kinetic energy. Thus, when these orbitals are filled with electrons, and this is the case for $D^{(-)}$, we get a barrier. Along the same argument we also understand that when the highest occupied state of $D^{(-)}$ is emptied, as is the case for the neutral or positively charged defect, the barrier should decrease or even vanish. In Fig. 16 we see indeed that for the neutral system the total-energy curve differs significantly from that of the negatively charged center. For $D^{(0)}$ the stable geometry would be at the tetrahedral position (zero displacement). However, at the V–I pair configuration we can still identify a local minimum. The barrier from this local minimum to the global minimum of $D^{(0)}$ is, however, much smaller than that of the $[D^{(-)} - e^-(E_F)]$ curve. We find that the calculated barrier heights depend sensitively on the **k** summation. Improving on the Γ-point approximation, Dabrowski and Scheffler (1992) estimated that the theoretical barriers for $D^{(0)}$ and $[D^{(-)} - e^-(E_F)]$ for a V–$I \rightarrow Si_{Ga}$ path would be about 0.1 and 0.5 eV, respectively.

The main effects of a change in the lattice constant are changes in the conduction band structure. Assuming that we have n-type conditions, this translates into a change of the Fermi level. As a consequence we obtain a (to first order) rigid shift of the $[D^{(+)} + e^-(E_F)]$ and the $[D^{(-)} - e^-(E_F)]$ curves relatively to the $D^{(0)}$ curve. The calculations also imply that the structural

transition from the C_{3v} to the T_d geometry can be also induced without pressure but by changing the Fermi level. If the Fermi level is high, the absolute minimum of the three curves shown in Fig. 16 will be that of the $[D^{(-)} - e^-(E_F)]$ curve. Thus, the negatively charged defect with its V–I geometry will be stabilized. If the Fermi level is low, the $[D^{(+)} + e^-(E_F)]$ curve shifts to lower energy and the $[D^{(-)} - e^-(E_F)]$ curve shifts to higher energy. Then the minimum of all three possible charge states is that of the positively charged Si substitutional. In Fig. 17 this discussion is summarized in a plot that shows the Fermi-level dependence of the different charge states. This figure also shows the theoretical level positions: The tetrahedral, substitutional Si has transition-state levels $\varepsilon_{Si_{Ga}}(+/0) = E_{CB} + 0.1\,\text{eV}$ and $\varepsilon_{Si_{Ga}}(0/-) = E_{CB} + 0.3\,\text{eV}$. Thus, at the lattice constant taken for the calculations in Figs. 16 and 17, both "levels" are resonances in the conduction band. For the V–I pair configuration, the results $\varepsilon_{V-I}(0/-) = E_{CB} - 0.5\,\text{eV}$ are obtained. As we are dealing here with transitions between a mainly valence-band derived state (the highest occupied state of the V–I geometry is essentially an As dangling orbital (Dabrowski and Scheffler, 1988a, 1989a, 1989b; Scheffler, 1989) and the conduction band, these transition-state energies, when compared to experimental ionization energies, may be subject to errors similar to those of the perfect crystal band gap. Figure 17 shows that the ground state for low Fermi energy is that of $D^{(+)}(Si_{Ga})$, and that the ground state for high Fermi energy is that of $D^{(-)}(V\text{–}I)$. The transition from $D^{(+)}(Si_{Ga})$ to $D^{(-)}(V\text{–}I)$ is direct, i.e., without passing through the neutral configuration. This is what is called a *negative U* behavior: In thermal equilibrium, there is either no electron in the defect-induced level, or there are

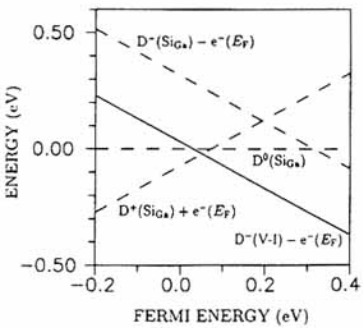

FIG. 17. Calculated total energies of the single positive, neutral, and single negative charged substitutional GaAs:Si_{Ga}, and of the single negative charged V–I pair as a function of the Fermi level, after Dabrowski and Scheffler (1992). $E_F = 0$ is the bottom of the conduction band. The lattice constant underlying these calculations is $a = 5.68$ Å, which corresponds to a pressure of -5 kbar in Fig. 15. The main approximations that may affect some quantitative results are the neglect of lattice relaxations and the replacement of the **k** summation by the Γ-point.

two electrons. The coulombic electron–electron repulsion, which typically implies that energy levels shift to higher energy when the occupation is increased, is more than compensated by the large lattice relaxation, i.e., by the displacement of the Si atom from the substitutional to the V–I pair configuration. The pressure dependence of the energy of the crossing point of the $D^{(+)}(Si_{Ga})$ and $D^{(-)}(V\text{–}I)$ lines of Fig. 17 is shown in Fig. 15 as the full line, labeled $\varepsilon(+/-)$. Figure 15 also shows the pressure dependence of the "normal" Si_{Ga} donor level, $\varepsilon_{Si_{Ga}}(+/0)$, as the dashed line.

Dabrowski and Scheffler (1992) compiled a list of the experimentally established properties of the Si DX center, and compared these properties to the properties implied by the theoretical results for the tetrahedral Si donor and the V–I pair. We will not repeat this discussion here, but we summarize that most of the experimental results are indeed consistent with the $Si_{Ga} \rightleftharpoons V\text{–}I$ model. However, the situation appears to be less clear than for the $EL2$ center. This is largely because most experiments were done for AlGaAs alloys for which the experimental analysis appears to be more complicated. On the other hand, the calculations were performed mainly for pure GaAs (Chadi and Chang, 1988a, 1988b; Dabrowski *et al.*, 1990; Dabrowski and Scheffler, 1992); only recently they were extended to alloys (Zhang, 1991).

Although the detailed calculations reported in Figs. 15–17 were concerned with cation-site donors, where the metastability is due to a displacement of the defect atom, we note that the same type of process can also occur for anion-site donors (Chadi and Chang, 1988a, 1988b). Here, however, the nearest neighbor cation moves.

Several experimental results are directly explained by the calculations. However, some questions remain that call for more accurate experiments as well as for more accurate calculations. The most severe disagreement between experiments and the properties of the V–I model comes from susceptibility measurements, which seem to indicate that DX centers are paramagnetic (Katchaturyan *et al.*, 1989). However, this result is not confirmed by EPR and in fact it has been questioned by other studies (Katsumuto *et al.*, 1990). Paramagnetism *of the ground state* of DX centers would be in conflict with the V–I model. A more detailed experimental and theoretical study of these points should help to finally confirm, to reject, or to refine the model.

Acknowledgment

The authors are grateful to J. Dabrowski and C. Ziegler for their critical reading of the manuscript.

REFERENCES

Bachelet, G. B., and Scheffler, M. (1985). *Proc. 17th Intl. Conf. Phys. Semiconductors* (Chadi, J. D., and Harrison, W. A., eds), p. 755.

Bachelet, G. B., Baraff, G. A., and Schlüter, M. (1981). *Phys. Rev. B* **24**, 915.

Bachelet, G. B., Hamann, D. R., and Schlüter, M. (1982). *Phys. Rev. B* **26**, 4199.

Bachelet, G. B., Jacucci, G., Car, R., and Parrinello, M. (1986). *Proc. 18th Intl. Conf. Phys. Semiconductors*, p. 801.

Baj, M., Dreszer, P., and Babinski, A. (1991). *Phys. Rev. B* **43**, 2070.

Bar-Yam, Y., and Joannopoulos, J. D. (1984). *Phys. Rev. Lett.* **52**, 1129; *Phys. Rev. B* **30**, 1844.

Baraff, G. A., and Lannoo, M. (1988). *Revue Phys. Appl.* **23**, 817.

Baraff, G. A., and Schlüter, M. (1978). *Phys. Rev. Lett.* **41**, 892.

Baraff, G. A., and Schlüter, M. (1979). *Phys. Rev. B* **19**, 4965.

Baraff, G. A., and Schlüter, M. (1984). *Phys. Rev. B* **30**, 1853.

Baraff, G. A., and Schlüter, M. (1985a). *Phys. Rev. Lett.* **55**, 2340.

Baraff, G. A., and Schlüter, M. (1985b). *Phys. Rev. Lett.* **55**, 1327.

Baraff, G. A., and Schlüter, M. (1986). *Phys. Rev. B* **33**, 7346.

Baraff, G. A., and Schlüter, M. (1987). *Phys. Rev. B* **35**, 6154.

Baraff, G. A., Kane, E. O., and Schlüter, M. (1979). *Phys. Rev. Lett.* **43**, 956.

Baraff, G. A., Kane, E. O., and Schlüter, M. (1980). *Phys. Rev. B* **21**, 3583.

Baraff, G. A., Lannoo, M., and Schlüter, M. (1988). "Defects in Electronic Materials," *Mater. Res. Soc. Symp. Proc. No. 104* (Stavola, M., Pearton, S. J., and Davies, G., eds.), p. 375. MRS, Pittsburgh.

Baroni, S., Gianozzi, P., and Testa, A. (1987). *Phys. Rev. Lett.* **58**, 1861.

Bäumler, M., Schneider, J., Kaufmann, U., Mitchel, W. C., and Yu, P. W. (1989a). *Phys. Rev. B* **39**, 6253.

Bäumler, M., Fuchs, F., and Kaufmann, U. (1989b). *Phys. Rev. B* **40**, 8072.

Beeler, F., Scheffler, M., and Andersen, O. K. (1985a). *Phys. Rev. Lett.* **54**, 2525.

Beeler, F., Andersen, O. K., and Scheffler, M. (1985b). *Phys. Rev. Lett.* **55**, 1498.

Beeler, F., Andersen, O. K., and Scheffler, M. (1990). *Phys. Rev. B* **41**, 1603.

Bergmann, K., Omling, P., Samuelson, L., and Grimmeiss, H. G. (1988). *Proceedings of the 5th Conference on Semiinsulating III-V Materials* (Grossmann, G., and Lebedo, L., eds.), p. 397. Hilger, Bristol.

Bernholc, J., Lipari, N. O., and Pantelides, S. T. (1978). *Phys. Rev. Lett.* **41**, 895.

Bernholc, J., Lipari, N. O., and Pantelides, S. T. (1980). *Phys. Rev. B* **21**, 3545.

Biernacki, S., and Scheffler, M. (1989). *Phys. Rev. Lett.* **63**, 290.

Biernacki, S., Scherz, U., Gillert, R., and Scheffler, M. (1989). *Mater. Sci. Forum* **38–41**, 625.

Blöchl, P. E. (1990). *Phys. Rev. B* **41**, 5414.

Blöchl, P. E., Van de Walle, C. G., and Pantelides, S. T. (1990). *Phys. Rev. Lett.* **64**, 1401.

Born, M., and Huang, K. (1954). *Dynamical Theory of Crystal Lattices*, p. 39. Oxford at the Clarendon Press.

Bourgoin, J. C., von Bardeleben, H. J., and Stiévenard, D. (1988). *J. Appl. Phys.* **64**, R65.

Caldas, M. J., and Fazzio, A. (1989). *Mater. Sci. Forum* **38–41**, 119.

Caldas, M., Dabrowski, J., Fazzio, J., and Scheffler, M. (1990). *Phys. Rev. Lett.* **65**, 2046.

Car, R., and Parrinello, M. (1985). *Phys. Rev. Lett.* **55**, 2471.

Car, R., Kelly, P. J., Oshiyama, A., and Pantelides, S. T. (1984). *Phys. Rev. Lett.* **52**, 1814.

Car, R., Kelly, P. J., Oshiyama, A., and Pantelides, S. T. (1985). *Phys. Rev. Lett.* **54**, 360.

Ceperley, D. M., and Alder, B. L. (1980). *Phys. Rev. Lett.* **45**, 566.

Chadi, D. J., and Chang, K. J. (1988a). *Phys. Rev. Lett.* **60**, 2187.

Chadi, D. J., and Chang, K. J. (1988b). *Phys. Rev. Lett.* **61**, 873.

Chadi, D. J., and Chang, K. J. (1989). *Phys. Rev. B* **39**, 10063.

Chantre, A., and Bois, D. (1985). *Phys. Rev. B* **31**, 7979.
Cohen, M. L. (1985). *Highlights in Condensed Matter Theory* (Bassani, F., Fumi, F., and Tosi, M. P., eds.), pp. 16–58. North-Holland, Amsterdam.
Dabrowski, J., and Scheffler, M. (1988a). *Phys. Rev. Lett.* **60**, 2183.
Dabrowski, J., and Scheffler, M. (1988b). *Proceedings of the 5th Conference on Semiinsulating III-V Materials* (Grossmann, G., and Lebedo, L., eds.), p. 37. Hilger, Bristol.
Dabrowski, J., and Scheffler, M. (1989a). *Phys. Rev. B* **40**, 10391.
Dabrowski, J., and Scheffler, M. (1989b). *Mater. Sci. Forum* **38–41**, 51.
Dabrowski, J., and Scheffler, M. (1992). *Proc. 16th Intl. Conf. on Defects in Semiconductors, Mater. Sci. Forum* **83–87** (G. Davis, ed.), p. 735. Trans Tech Publications, Switzerland.
Dabrowski, J., Scheffler, M., and Strehlow, R. (1990). *The Physics of Semiconductors* (E. M. Anastassakis and J. D. Joannopoulos, eds.), p. 489. World Scientific, Singapore.
Delerue, C., Lonnoo, M., and Stievenard, D. (1987). *Phys. Rev. Lett.* **59**, 2875.
Dreizler, R. M., and Gross, E. K. U. (1990). *Density Functional Theory*. Springer, Berlin, Heidelberg.
Fahy, S., Wang, X. W., and Louie, S. G. (1990). *Phys. Rev. Lett.* **65**, 1478.
Farid, B., and Needs, R. J. (1992). *Phys. Rev. B* **45**, 1067.
Figielski, T., and Wosinski, T. (1987). *Phys. Rev. B* **36**, 1269.
Fiorentini, V. (1992). *Phys. Rev. B* **46**, 2086.
Fleszar, A., and Gonze, X. (1990). *Phys. Rev. Lett.* **64**, 2961.
Frank, W. (1986). *Proceedings of the 12th International Symposium on GaAs and Related Compounds* (Fujimoto, M., ed.), p. 217. Hilger, Bristol.
Godby, R. W., Schlüter, M., and Sham, L. J. (1988). *Phys. Rev. B* **37**, 10159.
Gonze, X., and Vigneron, J.-P. (1989). *Phys. Rev. B* **39**, 13120.
Gonze, X., Käckell, P., and Scheffler, M. (1990). *Phys. Rev. B* **41**, 12264.
Gonze, X., Stumpf, R., and Scheffler, M. (1991). *Phys. Rev. B* **44**, 8503.
Gunnarsson, O., and Lundquist, B. I. (1976). *Phys. Rev. B* **13**, 4274.
Gunnarsson, O., Jepsen, O., and Andersen, O. K. (1983). *Phys. Rev. B* **27**, 7144.
Hamann, D. R., Schlüter, M., and Chiang, C. (1979). *Phys. Rev. Lett.* **43**, 1494.
Hedin, L. (1965). *Phys. Rev.* **139**, A796.
Hedin, L., and Lundqvist, S. (1969). *Solid State Physics* **23**, 2.
Heinemann, M., and Scheffler, M. (1991), unpublished.
Hjalmarson, H. P., Vogl, P., Wolford, D. J., and Dow, J. D. (1980). *Phys. Rev. Lett.* **44**, 810.
Hohenberg, P., and Kohn, W. (1964). *Phys. Rev.* **136**, 864.
Hybertsen, M. S., and Louie, S. G. (1986). *Phys. Rev. B* **34**, 5390.
Janak, J. (1978). *Phys. Rev. B* **18**, 7165.
Kamińska, M. (1987). *Phys. Scr. T* **19**, 551.
Kamińska, M., Skowronski, M., and Kuszko, W. (1985). *Phys. Rev. Lett.* **55**, 2204.
Katchaturyan, K. A., Awschalom, D. D., Rozen, J. R., and Weber, E. R. (1989). *Phys. Rev. Lett.* **63**, 1311.
Katsumoto, S., Matsunaga, N., Yoshida, Y., Sugiyama, K., and Kobayashi, S. (1990). *Proc. ICPS-20* (Anastassakis, E. M., and Joannopoulos, J. D., eds.), p. 481. World Scientific, Singapore.
Kerker, G. P. (1980). *J. Phys. C: Solid St. Phys.* **13**, L189.
King-Smith, R. D., Needs, R. J., Heine, V., and Hodgson, M. J. (1989). *Europhys. Lett.* **10**, 569.
Kleinman, L., and Bylander, D. M. (1982). *Phys. Rev. Lett.* **48**, 1425.
Kohn, W., and Sham, L. J. (1965). *Phys. Rev. B* **140**, A1133.
Krambrock, K., Spaeth, J.-M., Delerue, C., Allan, G., and Lannoo, M. (1992). *Phys. Rev. B* **45**, 1481.
Kröger, F. A. (1964). *The Chemistry of Imperfect Crystals*. North-Holland, Amsterdam.

Kuszko, W., Walzak, P. J., Trautmann, P., Kamińska, M., and Baranowski, J. M. (1986). *Mater. Sci. Forum* **10–12**, 317.

Laasonen, K., Nieminen, R. M., and Puska, M. J. (1992). *Phys. Rev. B* **45**, 4122.

Lagowski, J., Gatos, H. C., Kang, C. H., Skowronski, M., Ko, K. Y., and Lin, D. G. (1986). *Appl. Phys. Lett.* **49**, 892.

Landoldt-Börnstein (1982). *Numerical Data and Functional Relationships in Science and Technology*, New Series Group III, Vol. 17a and 22a, and references therein. Springer, New York.

Lang, D. V., Logan, R. A., and Jaros, M. (1979). *Phys. Rev. B* **19**, 1015.

Leung, T. C., Chan, C. T., and Harmon, B. N. (1991). *Phys. Rev. B* **44**, 2923.

Levinson, M., and Kefalas, J. A. (1987). *Phys. Rev. B* **35**, 9383.

Levy, M. (1982). *Phys. Rev. A* **26**, 1200.

Lundqvist, S., and March, N. H. (eds.) (1983). *Theory of the Inhomogeneous Electron Gas.* Plenum, New York.

Martin, G. M. (1981). *Appl. Phys. Lett.* **39**, 747.

Martin, G. M., and Makram-Ebeid, S. (1986). *Deep Centers in Semiconductors* (Pantelides, S. T., ed.), p. 399. Gordon and Breach, New York.

Meyer, B. K. (1988). *Revue Phys. Appl.* **23**, 809.

Meyer, B. K., Hofmann, D. M., and Spaeth, J.-M. (1986). *Mater. Sci. Forum* **10–12**, 311.

Meyer, B. K., Hofmann, D. M., Niklas, J. R., and Spaeth, J.-M. (1987). *Phys. Rev. B* **36**, 1332.

Mochizuki, T., and Ikoma, T. (1987). *Phys. Rev. Lett.* **59**, 590.

Moruzzi, V. L., Janak, J. F., and Williams, A. R. (1978). *Calculated Electronic Properties of Metals.* Pergamon Press, New York.

Nissen, M. K., Steiner, T., Beckett, D. J. S., and Thewalt, M. L. W. (1990). *Phys. Rev. Lett.* **65**, 2282.

Nissen, M. K., Villemaire, A., and Thewalt, M. L. W. (1991). *Phys. Rev. Lett.* **67**, 112.

Overhof, H., Scheffler, M., and Weinert, C. M. (1991). *Phys. Rev. B* **43**, 12494.

Pantelides, S. T. (1978). *Rev. Mod. Phys.* **50**, 797.

Perdew, J. P., and Levy, M. (1983). *Phys. Rev. Lett.* **51**, 1884.

Perdew, J. P., and Zunger, A. (1981). *Phys. Rev. B* **23**, 5048.

Sajovec, F., Wolf, R., Fattah, A., Bickmann, K., Wenzl, H., Nagel, G., Rüfer, H., Tomzig, E., and De Bièvre, P. (1990). *Phys. Stat. Sol. (a)* **122**, 139.

Scheffler, M. (1982). *Advances in Solid State Physics* **22**, 115.

Scheffler M. (1988). *Physics of Solid Surfaces 1987*, edited by Koukal, T. p. 115, Elsevier, Amsterdam.

Scheffler, M. (1989). *Advances in Solid State Physics* **29**, 231.

Scheffler, M. and Dabrowski, J. (1988). *Phil. Mag.* **A58**, 107.

Scheffler, M., and Scherz, U. (1986). *Mater. Sci. Forum* **10–12**, 353.

Scheffler, M., Vigneron, J. P., and Bachelet, G. B. (1982). *Phys. Rev. Lett.* **49**, 1765.

Scheffler, M., Beeler, F., Jepsen, O., Gunnarsson, O., Andersen, O. K., and Bachelet, G. B. (1984). *Proceedings of the 13th International Conference on Defects in Semiconductors*, edited by Kimerling, L. C., and Parsey Jr., L. M. (*The Metallurgical Society of AIME*), p. 45, New York.

Scheffler, M., Vigneron, J. P., and Bachelet, G. B. (1985). *Phys. Rev. B* **31**, 6541.

Schlüter, M. (1987). *Third Brazilian School of Semiconductor Physics* (Gonçalves da Silva, C. E. T., Oliveira, L. E., and Leite, J. R., eds.), p. 196.

Sham, L. J., and Kohn, W. (1966). *Phys. Rev. B* **145**, 561.

Sham, L. J., and Schlüter, M. (1983). *Phys. Rev. Lett.* **51**, 1888.

Slater, J. C. (1974). *The Self-Consistent Field for Molecules and Solids.* McGraw-Hill, New York.

Trautmann *et al.* (unpublished).

Vandebilt, D. H. (1990). *Phys. Rev. B* **41**, 7892.
van Kooten, J. J., Weller, G. A., and Ammerlaan, C. A. J. (1984). *Phys. Rev. B* **30**, 4564.
von Bardeleben, H. J., Stiévenard, D., Bourgoin, J. C., and Huber, A. (1985). *Appl. Phys. Lett.* **47**, 970.
von Bardeleben, H. J., Stiévenard, D., Deresmes, D., Huber, A., and Bourgoin, J. C. (1986). *Phys. Rev. B* **34**, 7192.
Wager, J. F., and Van Vechten, J. A. (1987). *Phys. Rev. B* **35**, 1269.
Watkins, G. D. (1989). *Mater. Sci. Forum* **38–41**, 39.
Watkins, G. D., and Troxell, J. R. (1980). *Phys. Rev. Lett.* **41**, 593.
Weast, C. R. (ed.) (1986). *Handbook of Chemistry and Physics*. Chemical Rubber Company, Boca Raton, Florida.
Weber, E. R., and Omling, P. (1985). *Advances in Solid State Physics* **25**, 623.
Wenzl, H., Mika, K., and Henkel, D. (1990a). *J. Crystal Growth* **100**, 377.
Wenzl, H., Mika, K., and Henkel, D. (1990b). *Cryst. Res. Technol.* **25**, 699.
Wenzl, H., Dahlen, A., Fattah, A., Petersen, S., Mika, K., and Henkel, D. (1991). *J. Crystal Growth* **109**, 191.
Wenzl, H., Oates, W. A., and Mika, K. (1992). *Handbook of Crystal Growth* (Hurle, D. T. J., ed.).
Zhang, S. B. (1991). *Phys. Rev. B* **44**, 3417.
Zhang, S. B., and Chadi, D. J. (1990). *Phys. Rev. B* **42**, 7174.
Ziegler, C., and Scherz, U. (1992). *Mater. Sci. Forum* **83–87**, 929.
Ziegler, C., *et al.* (1993).